Advanced SYNCOM

November 1962

MONTHLY PROGRESS REPORT

•

NASA Contract 5-2797
SSD 2574R

AEROSPACE GROUP
SPACE SYSTEMS DIVISION
HUGHES AIRCRAFT COMPANY
CULVER CITY, CALIFORNIA

HUGHES

HUGHES AIRCRAFT COMPANY

AEROSPACE GROUP

SPACE SYSTEMS DIVISION

CULVER CITY, CALIFORNIA

15 December 1962

SUBJECT: Advanced Syncom Monthly Report for November 1962

TO: Mr. Alton E. Jones
             Program Manager, Syncom
             Goddard Space Flight Center
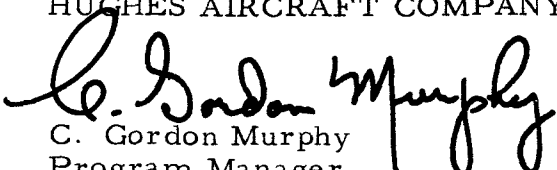   Code 621
             Greenbelt, Maryland

Attached are copies of the Advanced Syncom Monthly Progress Report for November 1962.

The dual-mode transponder detailed circuit designs were well under way at the close of the reporting period, with fabrication of several of the units completed and testing in process.

The traveling-wave tube was assembled to the package stage. Data obtained from tube No. 384H-7 while in the prepackaged stage showed optimum performance at 4.0 kmc with more than 2.5 watts of power out. This tube exhibited excellent collector depression and the beam efficiency exceeded 37 percent at the above power level.

Proposals from seven potential subcontractors for the hot gas system are under evaluation. The competence demonstrated by the proposals is generally high and the proposed systems confirm that the Syncom II requirements are within the state of the art in the hot gas industry.

HUGHES AIRCRAFT COMPANY

C. Gordon Murphy
Program Manager
Project Syncom

cc: H.E. Tetirick
     Goddard Space Flight Center
     Code 241
     Greenbelt, Maryland

Advanced SYNCOM

November 1962

MONTHLY PROGRESS REPORT

●

NASA Contract 5-2797
SSD 2574R

CONTENTS

APPENDIX A.   BENDIX PHOTODETECTOR FOR
SYNCOM ATTITUDE REFERENCE

1. INTRODUCTION

Under NASA Goddard Space Flight Center Contract NAS-5-2797, Hughes Aircraft Company is conducting feasibility studies and advanced technological development for an advanced, stationary, active repeater, communication satellite.

An Initial Project Development Plan, submitted to Goddard on 15 August 1962, reported the initial system feasibility studies and delineated technical approaches, the administrative plan, manpower requirements, schedule, and funding considerations appropriate for accomplishing the NASA contract objectives.

These monthly technical letter reports present the technical progress made during the reporting period, the critical problems or delays encountered, and the plans for the forthcoming reporting period.

Separate reports of schedule status are provided through biweekly PERT reports. Monthly financial management reports provide the funding status.

2. SYSTEM DESIGN STUDY

SPACECRAFT DYNAMICS

Studies are under way to optimize the dynamic tradeoffs between the capability of the spin-rate control mechanism, the permissible tolerances on hot gas jet and apogee motor thrust vector misalignments, and the contributions by the various subsystems to spacecraft dynamic unbalance. It is expected that these studies will permit the initial specifications for the apogee motor physical tolerances to be relaxed.

LAUNCH AND ORBIT CONSIDERATIONS

The Lockheed Missiles and Space Company (LMSC) has completed a final report (30 September 1962) of their studies for launching Syncom II using the Atlas-Agena D. When this report is released for distribution, appropriate portions of Section 5 of the Initial Project Development Plan, Advanced Syncom, will be revised to reflect the LMSC study results. The sections requiring updating include the ascent trajectory, transfer orbit, guidance error estimates, and Table 5-3, orbit dispersions.

USE OF POLARIS REFERENCE FOR ATTITUDE CONTROL

A preliminary examination was made to determine the feasibility of using a photodetector and a nonmechanical scanning system, proposed by the Eclipse-Pioneer Division, Bendix Corporation, as a body-mounted detector of the star Polaris. The Polaris tracker would provide a more precise attitude reference for Syncom.

The brief studies, detailed in Appendix A, show that it is feasible to adapt the Bendix photodetector with reasonably sized optics, for use in Syncom II to locate Polaris and that attitude error may be determined by telemetering the video content of the star field for ground-based comparison with ephemerides of Polaris and local sun. System studies, including the tradeoffs between increased complexity and system improvement, would be required before a decision could be made.

SYSTEM RELIABILITY

Design Analyses

A preliminary design analysis of the phased-array antenna subsystem and control system fire angle generator has been performed and a reliability block diagram for the present concept developed (Figure 2-1). This analysis, though not complete, has included a compilation of parts count information for each circuit and an investigation of circuit redundancy, derating, duty factor, and failure mode characteristics. A reliability estimate for one quadrant of this subsystem would be of little value and would yield a pessimistic survival probability if only the parts count data were considered; i.e., if all components were required to operate for system success (a series event) with a 100-percent duty cycle. Such an estimate would be invalid and indicative only of the relative complexity of this subsystem, > 3700 parts per quadrant with an average failure rate equal to 0.012 percent per 1000 hours. Therefore, a reliability estimate for the control that accurately represents the logic must also accommodate those functions within the subsystem that have a low duty cycle, partial redundancy, or upon failure result only in a degradation in performance. A prediction of mission success will be presented when these conditions are delineated in sufficient detail to make a representative analysis.

As Figure 2-1, shows, the antenna phase control electronics are divided into two primary circuit functions: the digital control circuits, which generate the antenna phase reference signals, and the analog drive circuits, which receive the phase reference signals and convert them to analog form to provide excitation for the ferrite phase shifters to control the direction of the phased-array antenna beam. The digital control and analog drive circuits consist of approximately 2100 and 1500 electronic components respectively.

The digital control circuits for each quadrant include a circuit to synchronize the system with the spacecraft spinrate, a fire angle generator, a variable phase control to permit adjustment of beam center location, and a sine wave generator subassembly. The synchronizing loop incorporates a coarse slew adjustment for spacecraft spin speed correction that operates for a maximum of 2 minutes upon initial injection into orbit; after this maneuver it will operate whenever a large spin speed correction is made or alternate control electronic quadrants are selected. Loss of this function will only slightly degrade performance unless a catastrophic failure causes a continuous slew. A failure mode analysis to be performed during this program will determine and minimize in the design the probability of occurrence of such a catastrophic failure. The variable phase control has circuitry to accommodate ground command correction of the antenna beam direction. This correction will occur approximately at 1-week intervals, with a duration of 1 to 2 minutes. The sine wave generator operates at 100-percent duty cycle. It has been found that the recommended 90-percent derating factor has been applied where practicable within the digital electronics.
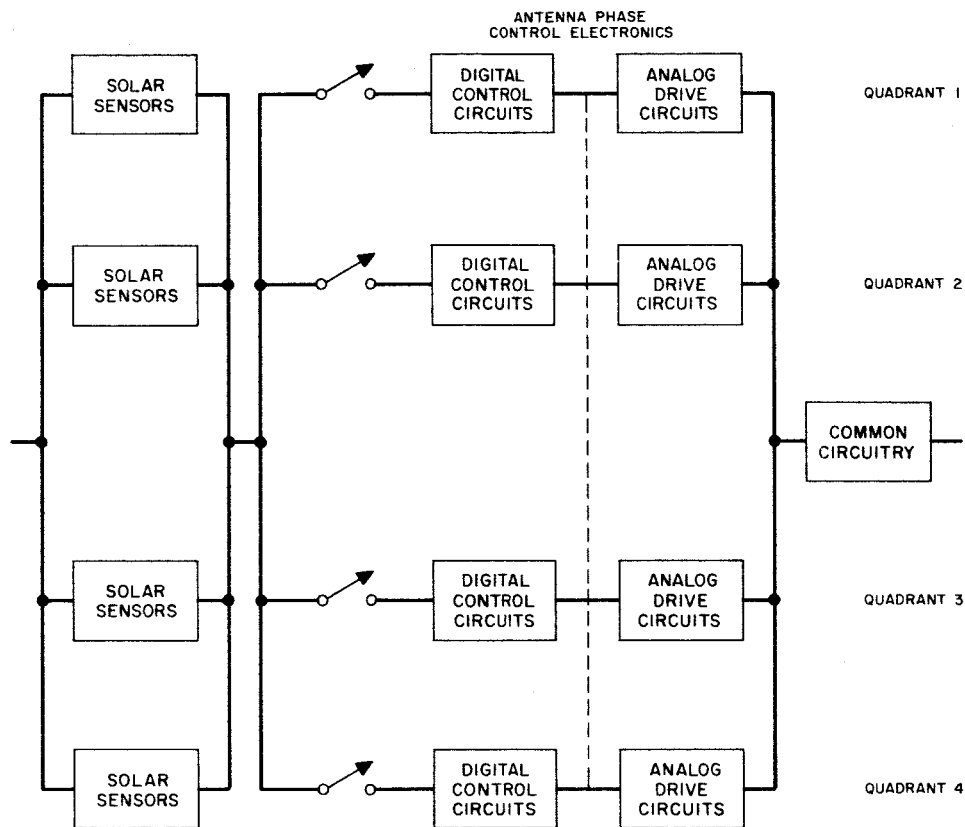
Figure 2-1. Phased-Array Antenna Subsystem
Reliability Block Diagram

The analog drive circuits include a summing network, which derives eight signals phase shifted approximately 22.5 degrees from the input sine wave, and eight pairs of waveform generators, each with one power amplifier. Investigation of this portion of the subsystem indicates that complex redundancy exists, and a failure of the control excitation to the phasing circuit to one or more of the 16 antenna elements will cause a degradation in performance and not a catastrophic failure. The RF would continue to be supplied to the element. Laboratory tests are currently being performed to determine the antenna system failure modes and the loss effect of antenna elements upon subsystem performance. These tests should result in criteria for incorporating degradation effects in the reliability mathematical model.

Specific recommendations have been made to enhance the reliability of the phased-array antenna subsystem. Emphasis has been placed upon reliability improvement of the power amplifier circuits, which have a minimum or no derating of components, through simplification and redundancy techniques.

A recommendation based upon these preliminary studies has been made suggesting that interquadrant paralleling of functions within the subsystem be considered as indicated in Figure 2-1 by the dashed lines. This redundancy technique can be accommodated prior to sine wave generator subassembly.

The solar sensor arrangement shown in Figure 2-1 is desirable so that all sensors will supply inputs to all electronics packages, provided the additional circuit complexity for isolation can be held to a minimum and a reasonable reliability improvement in the overall subsystem can be achieved.

System Studies

Probabilistic models for spacecraft availability and replacement rate have been developed. (See Section 5, where a summary of the steps in mathematical development is presented.)

The probability of a spacecraft failure prior to, during, and after replacement are characterized by three failure modes. The formulation of the utilization, outage, and duplication times yields equations that describe the fraction of useful time (up-time ratio or availability), of nonuseful time (down-time ratio), and of duplication time. Mathematical models for the number of satellites needed and replacement rate are presented. Numerical estimates of availability and replacement rate for one spacecraft based upon the probability of survival of at least one of four communications quadrants illustrate the models.

The fourfold redundancy and stepwise quadrant degradation of the Syncom II spacecraft make it possible, by proper choice of replacement decision criteria, to reduce the frequency of catastrophic communication failures. A study of the availability function for several decisions to replace

criteria is being performed to optimize availability and minimize the replacement rate. It is apparent from the probabilistic models that a significant gain will be achieved by minimizing the actual time to replace and maximizing the booster and launch sequence reliabilities.

An examination of the availability for a three spacecraft system will be initiated. Methods for utilizing the replaced spacecraft until its complete failure are contemplated. The analysis presented shows that one active satellite per orbital location is required; i.e., there does not seem to be any reason to have a continuous standby spacecraft at this time. However, the system queuing problem for utilization of launch facilities is pertinent to the cost effectiveness and is being considered as an extension of this analysis.

TEST EQUIPMENT

Frequency Translation Transponder Tests

Table 2-1 is a preliminary list of tests and equipment. The only item of equipment that may be specially designed and built for the test of the frequency translation transponder will be the communications panel(s). A block diagram of this panel is shown in Figure 2-2. Since there are four frequency translation transponders per spacecraft and each of them operates at a different frequency, some duplication of equipment is required. It may prove most feasible to have four panels, one for each spacecraft quadrant. As a minimum, the master oscillator crystal and the high pass output filter must be duplicated, the latter in order to eliminate necessity of readjusting the filter each time.

The frequency multipliers will probably not operate over a wide enough band to allow a single set to be used for all four quadrants. If this should prove to be the case, it would be necessary to construct four separate panels (one for each quadrant). These panels would contain the master oscillator, multiplying chains, and other microwave signal generation equipment except for the traveling-wave tube and power meter. The IF amplifier, phase detector, phase modulator, low-pass filter, and phase-lock status readouts would be placed on a separate chassis to be shared by the four quadrant RF panels. The commercial test equipment (TWT, power meter, TV signal generator, TV monitor, 35-75 megacycle signal generator) would also be used on a sharing basis.

Since testing of the transponder's multiple access mode requires generation of single sideband signals and linear amplification, there is little to be gained from combining the multiple access mode equipment into the same panels as the frequency translation mode equipment, particularly since their separation makes the equipment more versatile.

The feasibility of generating wide-band phase-modulated signals at 54 megacycles has not yet been studied. The relatively simple system shown

2-5

Figure 2-2. Communication Test Equipment for Frequency
Translation Mode of Syncom II Transponder

TABLE 2-1. FREQUENCY TRANSLATION TRANSPONDER TESTING

Parameter to be Tested	Test Equipment Required	Comments
1) Input and output frequencies and bandwidths (including IF)	Communications panel, 35 to 75 mc signal generator, transfer oscillator, electronic counter and frequency converter, TV signal generator, TV monitor, and spectrum analyzer.	Block diagram of communications panel is shown in Figure 2-2.
2) Image rejection	Same as above	Spectrum analyzer would be used to receive and measure transponder outputs in response to image inputs.
3) Power output	RF power meter	
4) Sensitivity	Same as 1	Phase-locked loop status would be monitored as a function of signal level.
5) Signal distortion (intermodulation, phase distortion, etc.)	Same as 1	Distortion checks would be made by viewing TV patterns on TV monitor on inputs and outputs of transponder.

on the block diagram may not prove operable; if so, the alternate plan indicated on the block diagram is a standard technique and should not present any serious technical difficulties.

Spacecraft hardware (in either spacecraft or a repackaged form) can be used for the following items:

1) Master oscillator

2) Frequency multipliers

3) Hybrids and isolators

The decision to use spacecraft parts will have to be made on the basis of its effect on cost and schedules.

SSB/PM Multiple Access Transponder Tests

Preliminary system tests and equipment for the SSB/PM multiple access transponder tests listed in Table 2-2 will be designed to simulate ground station operation as well as to system-test the transponder. Figure 2-3 is a preliminary block diagram of the SSB/PM multiple access transponder test equipment.

TABLE 2-2. SSB/PM MULTIPLE ACCESS TRANSPONDER TESTING

System Test	Test Equipment Required
Receiver sensitivity or minimum readable signal level and dynamic range	Test SSB generator and PM receiver (similar to ground station), spectrum analyzer, oscilloscope, power meter
Transponder bandwidth	Test SSB generator and PM receiver, spectrum analyzer, oscilloscope
Phase modulation index	Test SSB generator and PM receiver, spectrum analyzer
Power output	Test SSB generator and PM receiver, power meter, spectrum analyzer
Intermodulation distortion	Noise generator, narrow-band reject filter, test SSB generator and PM receiver, spectrum analyzer
Noise figure (if test access permits)	Noise tube and noise meter

Antenna Control System Tests

Tests of the antenna control system may be made with the satellite either stationary or rotating. Table 2-3 lists the required preliminary tests and equipment; block diagrams for these tests are given in Figures 2-4 and 2-5.
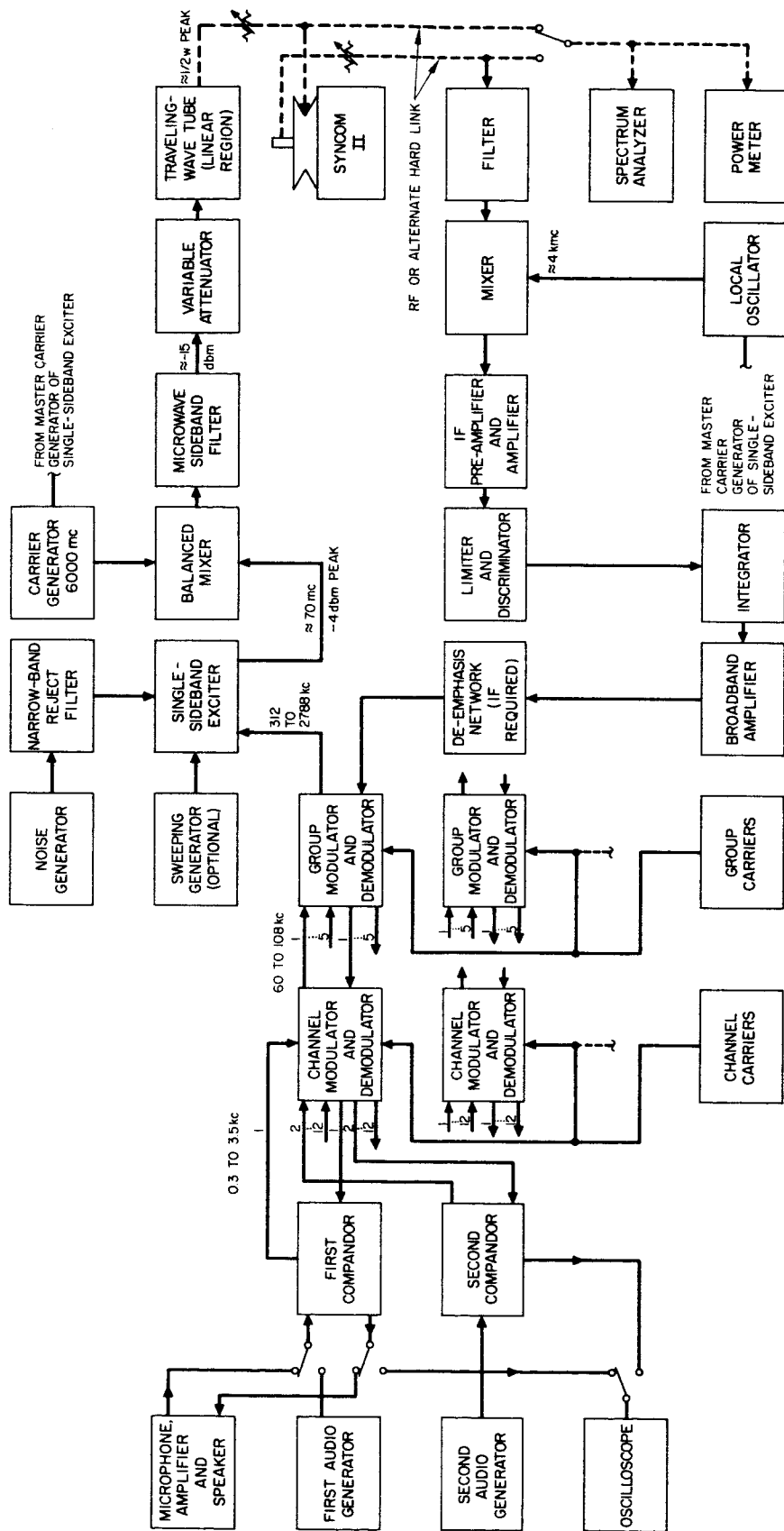
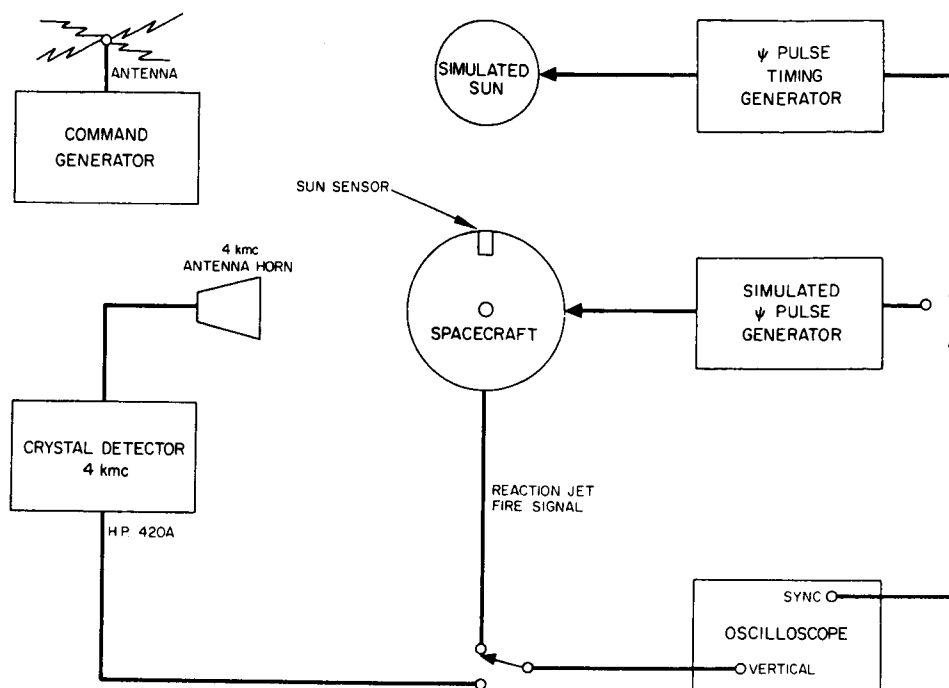Figure 2-3. Test Equipment for Multiple-Access Mode of Syncom II Transponder

Figure 2-4. Antenna Control System Tests
with Nonrotating Spacecraft
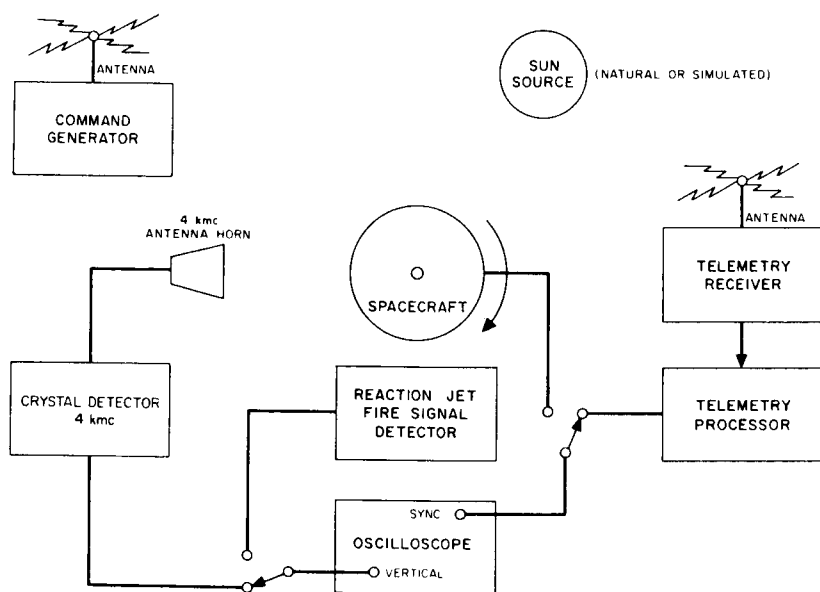
Figure 2-5. Antenna Control System Tests
with Rotating Spacecraft

2-10

TABLE 2-3. ANTENNA CONTROL SYSTEM TESTING

System Test	Equipment
1) Stationary spacecraft	
a) Antenna radiation pattern is de-spun in synchronism with the ψ-pulse, has 24-hour angular correction, and responds to external commands.	4-gc antenna horn, antenna horn stand, 4-gc crystal detector (HP 420A), oscilloscope (TKX545)
b) Reaction jet fire signal occurs at correct angular position and with correct pulse width.	Plug-in preamplifier (TKX Type C/A), pulse generator.
2) Rotating spacecraft	
a) External commands control angular position of antenna radiation pattern.	4-gc antenna horn, 4-gc crystal detector (HP 420A),
b) Antenna radiation pattern reverts to "pancake" shape.	antenna horn stand, oscilloscope (TKX545), Plug-in preamplifier (TKX Type C/A),
c) Reaction jet fire signal occurs at correct angular position and with correct pulse width.	command generator, telemetry receiver, reaction jet fire signal detector, spin table.

3. ADVANCED TECHNOLOGICAL DEVELOPMENT

DUAL-MODE TRANSPONDER

Circuits Common to Frequency Translation and Multiple Access Transponders

Dual Mixer (6390-6336/6357 mc). Drawings have been prepared of the stripline circuits and base plates for the dual mixer, which operates approximately 1000 mc below that of Syncom I. The hardware development has included completion of a test fixture to permit optimization of the match of the two mixer diodes, RF choke, RF filter, and the RF hybrid ring. Three alternate materials, revolite, tellite, and duroid, will be tested for the hybrid rings to minimize losses and simplify fabrication processes.

Hybrid (4170 mc). Drawings of the 4170 mc hybrid have been completed and fabrication of the hardware initiated. The results of the alternate material tests conducted for the dual mixer stripline will be applied to the hybrid.

RF Power Switch. The center frequency of the RF power switch under test during the previous report period was measured to be 3700 mc, with static losses between 0.15 and 0.20 db over a 5-percent band. Current effort is directed toward scaling the center frequency to 4080 mc and decreasing the peak current pulse required to switch the magnetic field from 3 to less than 1 ampere.

X32 Multiplier. Three X32 multipliers have been fabricated and tested. These multipliers have the same varactor diodes used in Syncom I (See Figure 3-1).

X2 Multiplier. A breadboard 2 to 4 kmc doubler has been developed and is undergoing tests to finalize the configuration prior to fabrication of the engineering model (Figure 3-2).

X3 Multiplier. Circuit development for the X3 multiplier has been initiated. The circuit will be fabricated and tested during the next report period.
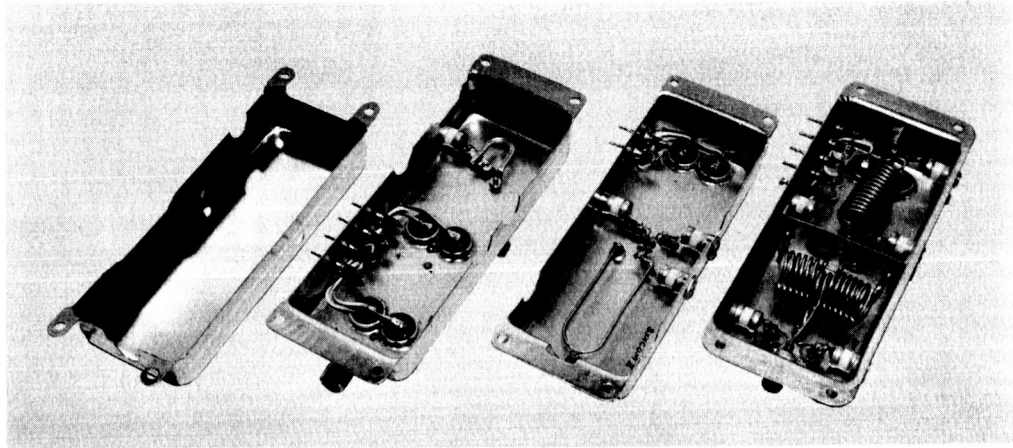
a) Exploded View, Interior
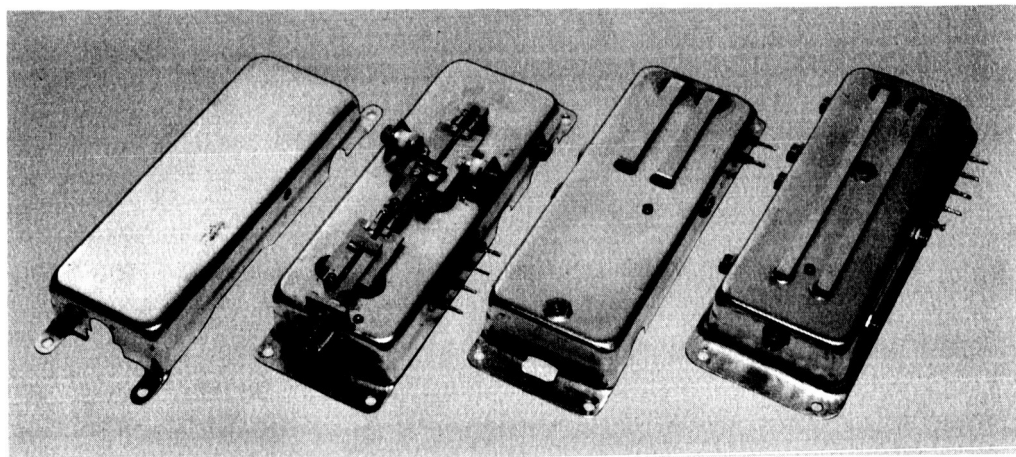
b) Exploded View, Exterior
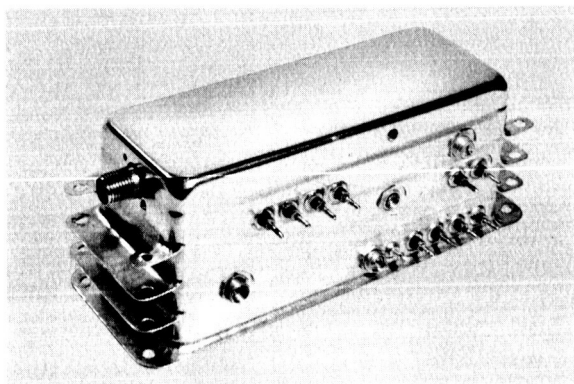
c) Assembled

Figure 3-1. X32 Multiplier
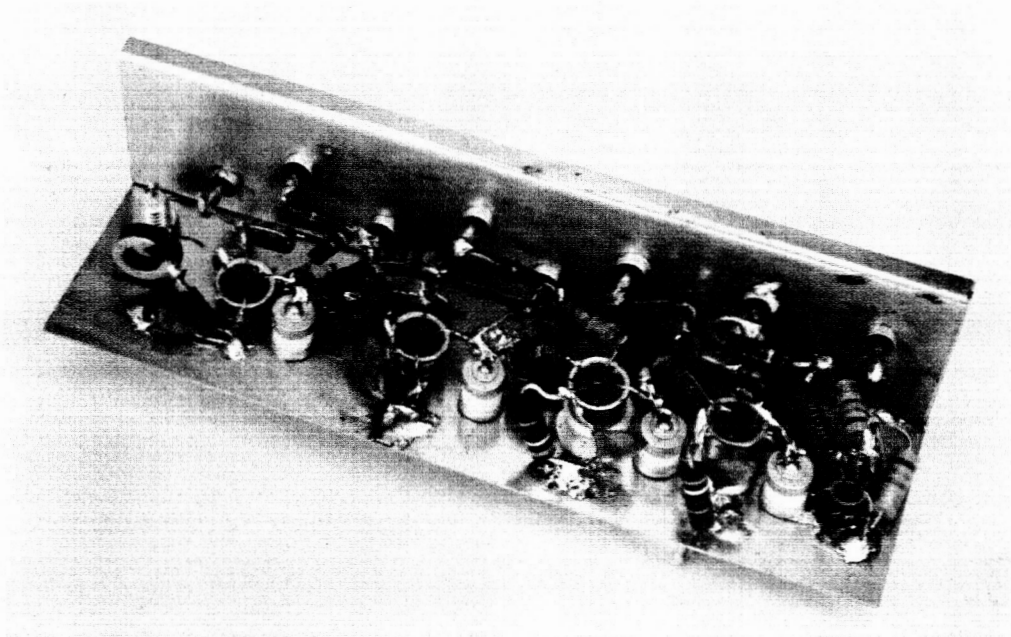
a) Circuit Side
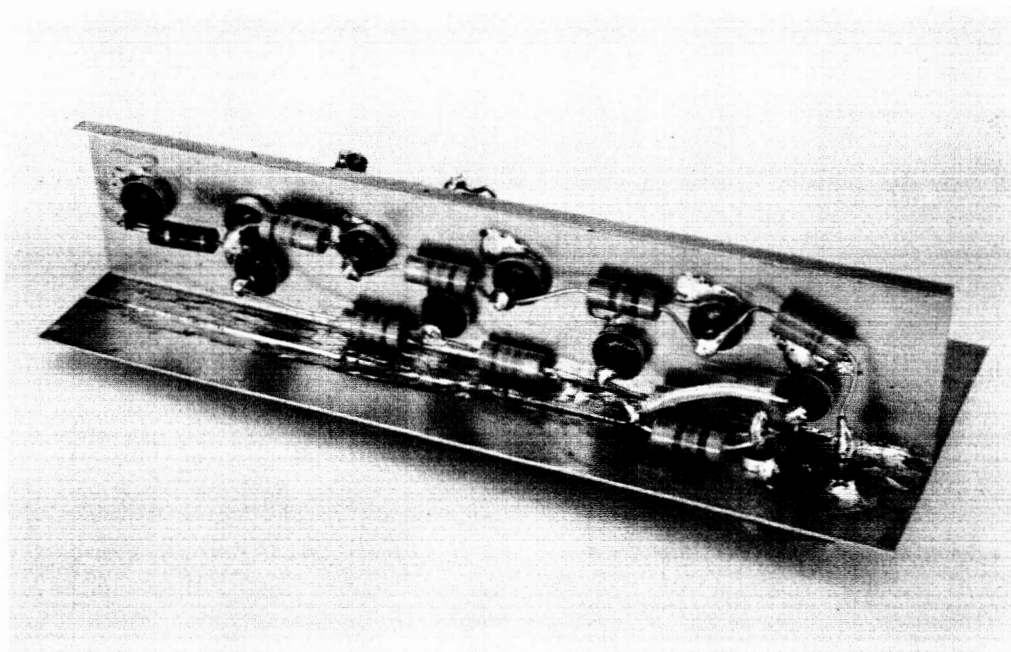
b) Power Supply Decoupling Circuit Side

Figure 3-2. X2 Multiplier and Amplifier

Circuits for FM Frequency Translation Transponder

Preamplifier and IF Amplifier. Effort to date has been directed toward development of 25-mc bandwidth circuits applying the circuit techniques developed for Syncom I and using the same transistors. Some difficulty has been encountered with this transformer-coupled approach, and therefore a parallel consideration of an alternate transistor and RC-coupled circuits is under way.

High-Level Mixer. Hardware development of the high-level mixer has been initiated, using Syncom I techniques. An alternate mixer approach is being considered in parallel with this development; it has a varactor diode modulator as the first stage of a two-stage mixer. The required 4224-mc drive power is reduced sufficiently to permit a single (power level) design for all three X32 multiplier applications in the dual-mode transponder.

14 db Coupler (4224 mc). Design has been completed and drawings prepared for fabrication of a 14-db coupler.

Beacon Oscillator (144 mc). The 144-mc beacon oscillator has been fabricated and tested electrically. The circuits provide the desired 3 milliwatts at 144 mc.

Isolators (2112 mc). Parts fabrication has been completed and assembly of four 2112-mc isolators initiated. These units will be completed and tested during the December report period.

Dual-Filter Hybrid (2112 mc). A purchase order was released to Rantec to supply the 2112-mc dual-filter hybrid. Delivery of engineering model units is expected during the next report period. This hybrid is scaled from the 1849-mc dual-filter band of Syncom I, with the additional change of the level difference between the two output arms.

Dual-Single Sideband Filter-Diplexer (4080/4170 mc). A purchase order was released to Rantec to supply the 4080/4170 mc dual-single sideband filter-diplexer. Delivery of engineering model units is expected during the next report period. This filter-diplexer will select the 4170-mc modulation sideband from the high-level mixer and diplex this signal with the 4080-mc beacon signal.

Circuits for Multiple-Access Transponder

Phase Modulator (32.5 mc). The phase modulator has been fabricated and tested electrically. During the next report period it will be mated to the transmitter master oscillator and the preamplifier.

Receiver Master Oscillator (66.223 mc). The engineering model master oscillator has been fabricated and tested electrically. The power

output and frequency are satisfactory. Planned additional testing includes determination of the short term stability of this oscillator.

Doubler/Amplifier (32.5/65 mc). Breadboard circuits of the 32.5/ 65-mc doubler and amplifier have been prepared and are undergoing final development prior to incorporation into the engineering model.

Transmitter Master Oscillator (32.578125 mc). The engineering model transmitter master oscillator has been completed and tested electrically. During the next report period this oscillator will be mated with the phase modulator.

Filter-Isolator (2085 and 2119 mc). A purchase order was released to Rantec to supply the 2085- and the 2119-mc filters. Delivery of all engineering model units was completed and testing will be conducted during the next report period.

TRAVELING-WAVE TUBE

During this period tube No. 384H-7 was assembled to the packaged stage and tested. Four other tubes were scrapped because of an assembly error, but the cause of the error has been traced and corrected.

The test results from No. 384H-7 at the prepackaging stage showed the change in helix pitch raised the optimum performance frequency to about 4000 mc and the beam voltage enough to obtain a power output of over 2.5 watts at 4000 mc. The tube exhibited excellent collector depression and the efficiency was over 37 percent at this power output. The increase in helix pitch has lowered the gain, but a 15 percent increase in helix length should increase the gain to the desired value.

The data obtained from No. 384H-7 after packaging was not consistent. It is believed that the output match changed during packaging. Investigation is under way to determine the cause of the mismatch and the necessary action to correct it.

Preassembly work has begun on two tubes (384H-8 and -9) with the longer helix. These will be tested in December.

PHASED-ARRAY TRANSMITTING ANTENNA

Array Development, Vertical Polarization

The vertically polarized array was tested on the Hughes antenna range with the phased-array antenna test fixture, which uses cables cut to the proper length to give the necessary phase shifts for a static pattern. Both horizontal and vertical patterns were taken at a number of frequencies in the

band. The results at 3980, 4080, and 4180 mc are shown in Figure 3-3. The measured gain at 4080 mc was 15 db through the test fixture; with allowance for fixture attenuation and mismatch, the actual antenna gain is estimated at 17 db.

Since the receiving antenna feed passes up through the center of the transmitting array, a check was made on the effect of a rod in the center. With a solid conducting rod, the mainlobe gain decreased slightly less than 1 db and the first sidelobes increased approximately 1.5 db. When a number of quarter-wave RF chokes were placed on the rod, there was no measurable effect on the pattern in the vicinity of the mainlobe.

All the RF components for the breadboard antenna have been received and assembled to check the mechanical structure. The antenna is shown being assembled in Figure 3-4; Figure 3-5 illustrates a top view. The eight phase shifters are symmetrical, with the power divider on the bottom and the coaxial cables feeding the antenna at the top.

RF Circuits

Ferrites. Enough ferrites for the breadboard antenna have been received from Trans-Tech, Inc. Initial tests of these gave approximately the same results as tests of the earlier units, which appear to be satisfactory for this application.

Output Couplers. The output couplers have been completed and tested. They are in the form of a quarter-wave plate that converts circular polarization to linear polarization. The input signal to the output coupler is linearly polarized, but may be resolved into two counter-rotating circular polarizations. Thus one output couples to right-hand circular polarization, while the other output couples to left-hand circular polarization. In this way, rotation of the linearly polarized input results in a phase shift of each of the two outputs. Typical insertion loss was of the order of 0.5 db with 0.1 db variations as a function of input polarization.

Phase Shifters. All eight phase shifters have been assembled and are being tested. Figure 3-6 shows the parts of a phase shifter; the input coupler is on the right, the field coil in the center, and the output coupler on the left. In the foregound is the ferrite tube, with its teflon insert in front and the matching sections on either end. The output coupler can be rotated with respect to the input. It is adjusted so that the two outputs are in phase when there is no current in the field coil, to ensure an omnidirectional pattern if the phase shifters are turned off. With current in one winding of the coil, the coil can then be adjusted so that the two outputs are again in phase.

Power Splitter. The stripline eight-way power splitter was assembled and tested at 4080 mc. The power division from input to each of the eight outputs varied from 8.8 to 9.2 db. Thus there appeared to be negligible loss through the power splitter. The manner in which the output varied
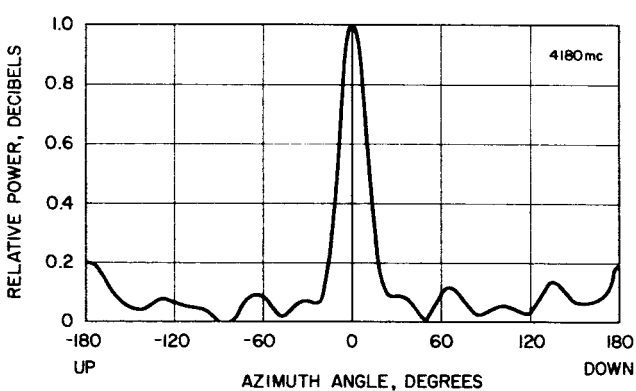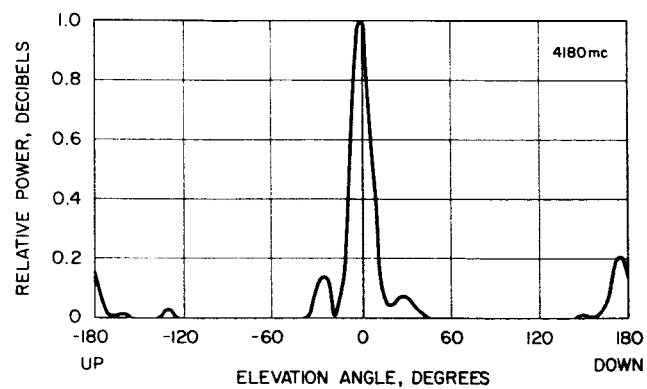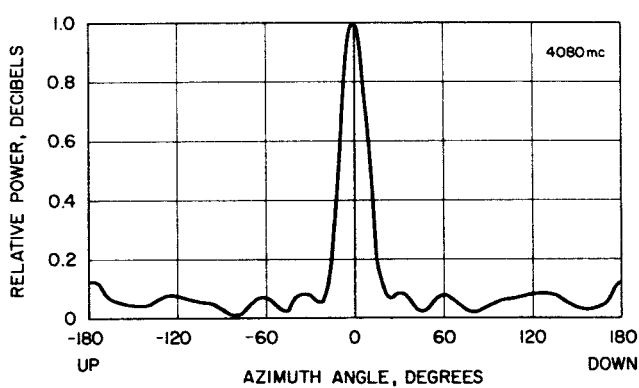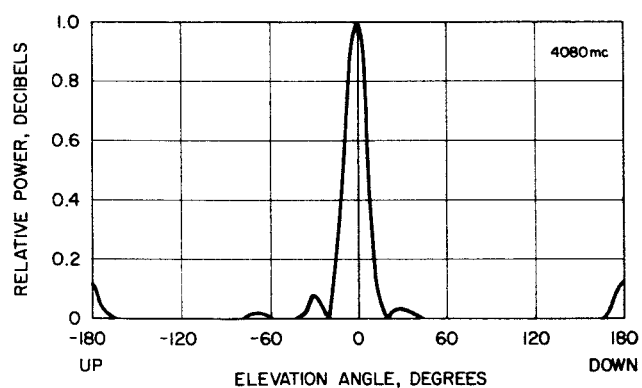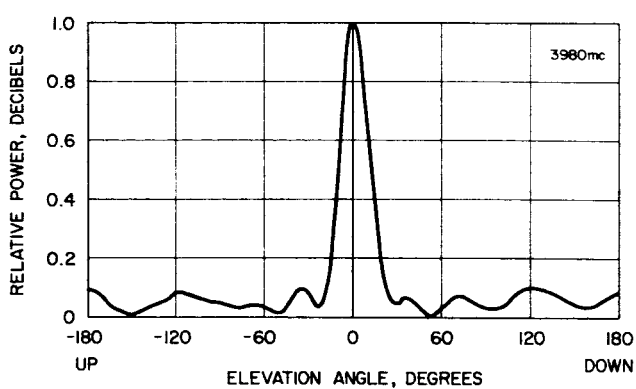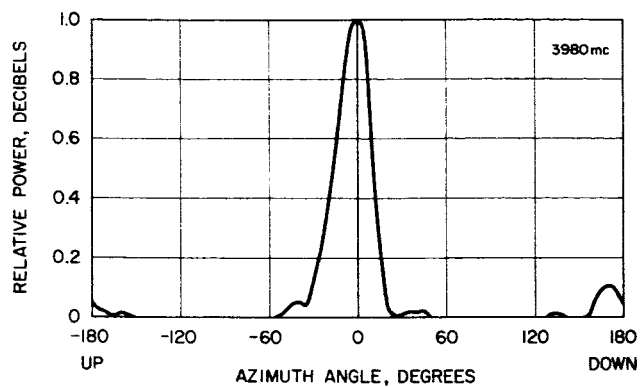
Vertical Plane   Horizontal Plane

Figure 3-3. Antenna Patterns of 4-kmc Phased-Array Antenna

3-7
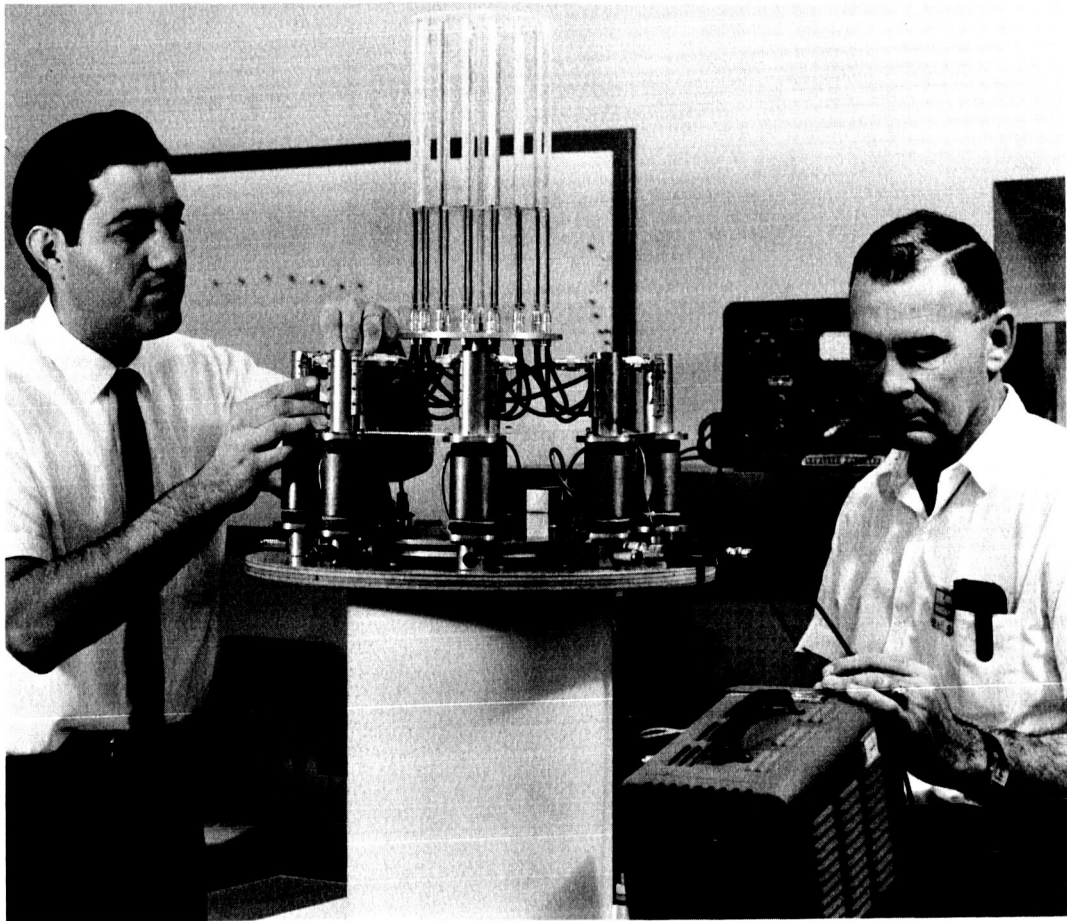
Figure 3-4. Phased-Array Antenna Assembly and Checkout
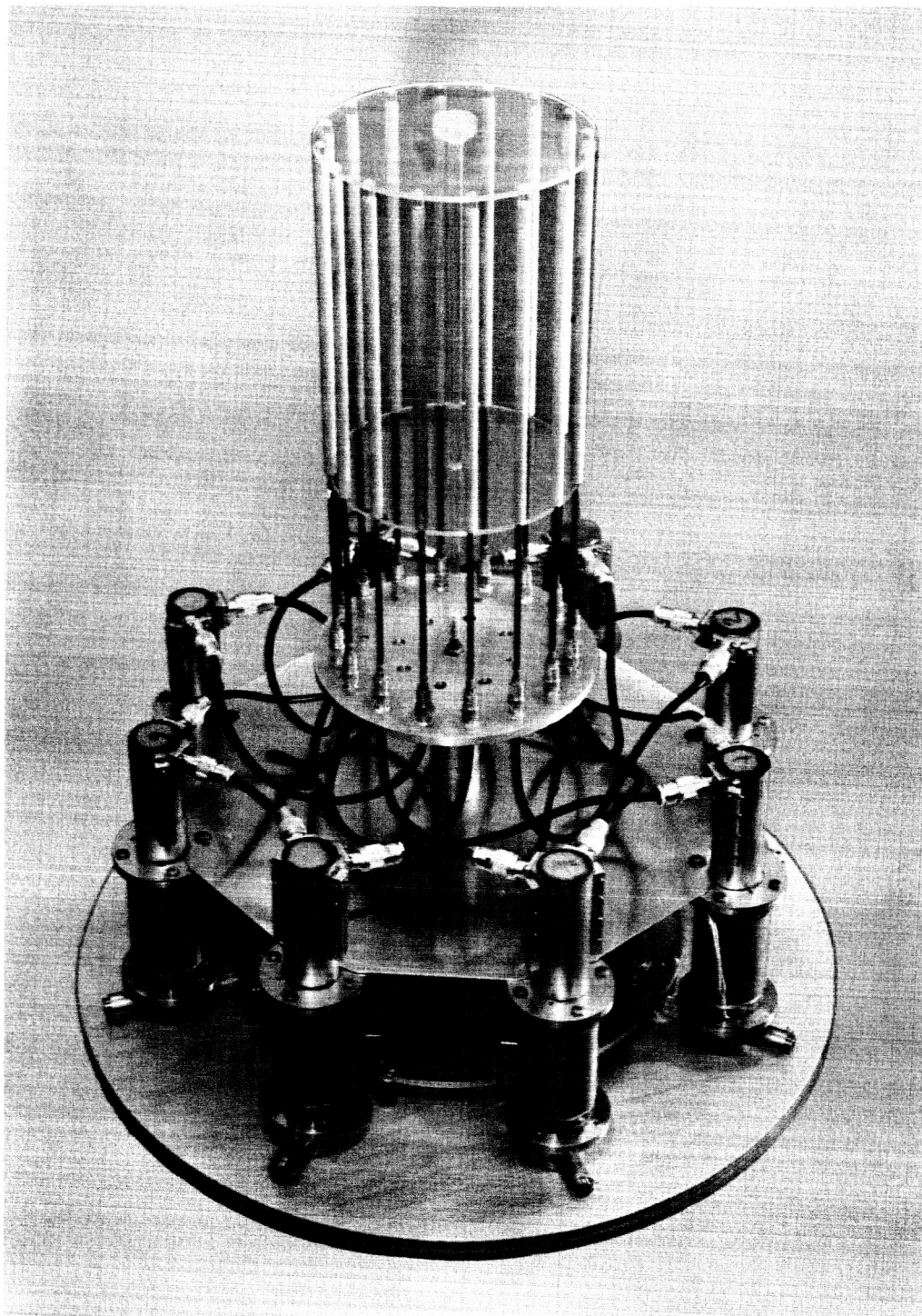
Figure 3-5. Phased-Array Antenna Complete Breadboard
Showing Phase Shifters Circumferentially Arranged
Around 16-Element Syncom II Antenna
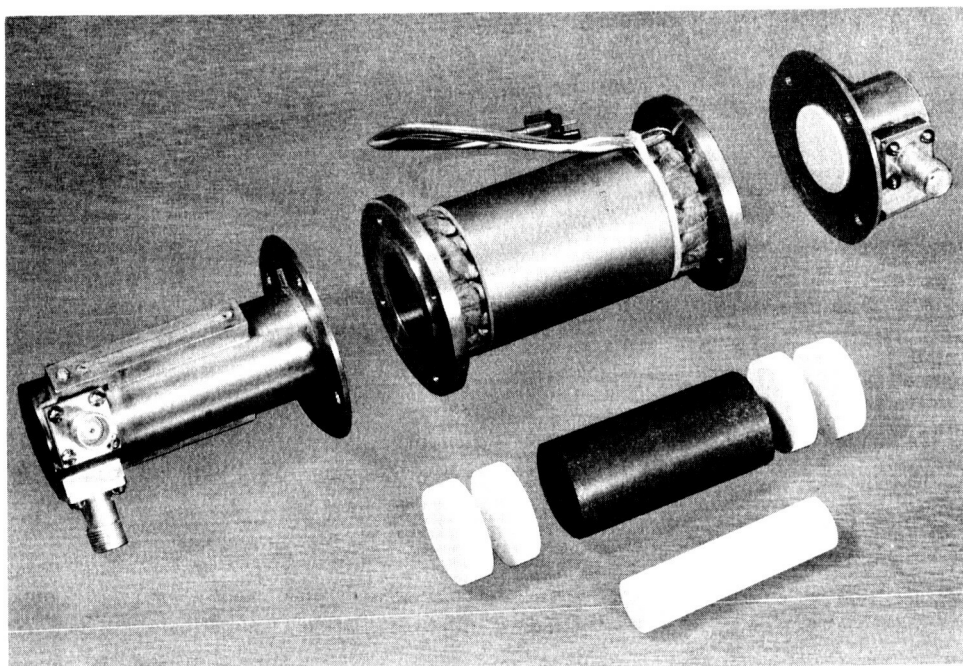
Figure 3-6. Exploded View of Breadboard Ferrite Phase Shifter
Used in Phased-Array Antenna System

seemed to indicate that the hybrid rings did not scale properly and may be tuned to an off-nominal frequency.

Stripline Circuits. Work is continuing on the stripline version of the antenna RF system, using a double-layer air dielectric stripline for the circuits between the phase shifters and the antenna elements. Layout for a number of the individual stripline components as well as the overall layout is in progress.

Control Electronics

Analog Electronics. The circuit design for the new waveform generating circuits described last month is complete. Sixteen plug-in boards, one for each of the two windings on each phase shifter field coil are being fabricated for use with the breadboard antenna. All parts have been ordered and most have been received. Each board has 10 transistors, 20 diodes, and 65 resistors. Figure 3-7 shows a simplified block diagram of the new circuits. The three sinusoidal inputs are supplied by the digital circuits; the adding network combines these to generate eight sine waves differing in phase by 22.5 degrees, each of which goes to two waveform generators. As shown, E_1 goes to a push-pull amplifier followed by diodes, thus acting like a full-wave rectifier and giving a transfer function to E_2 as indicated. The next amplifier is similar, except that the diodes are biased, resulting in a transfer function to E_3 as shown. Finally E_3 passes through a diode shaping network which rounds off the transfer function to E_4. The amplitude of the sinusoidal input at E_1 is adjusted to swing over the range indicated. The output passes through a driver amplifier and a power amplifier to the field coils. The other 15 channels are similar except for an extra diode and resistor in the eight that generate the sine output. The engineering model analog electronics will be combined with the digital electronics for package design.

Antenna Digital Control Electronics. Final releases of the digital control circuits, which include most of the antenna control electronics, were completed in early November. The analog circuits were completed about 20 November. Major functional blocks (phase-lock loop and sine-wave generator subassemblies) of the digital control electronics have been breadboarded and tested to verify their operational design parameters. Figures 3-8, 3-9, and 3-10 illustrate the test and checkout of these blocks.

Seventy-three flat cards of 28 types will be used to mount the circuits. Card design was 80 percent complete and component procurement 90 percent complete on 1 December. Card assembly was started on 15 November and is expected to be complete by early January.

During the demonstration of the phased-array antenna in the engineering model spacecraft, the antenna control electronics will be contained in two units which will be located in the apogee motor volume of the spacecraft.
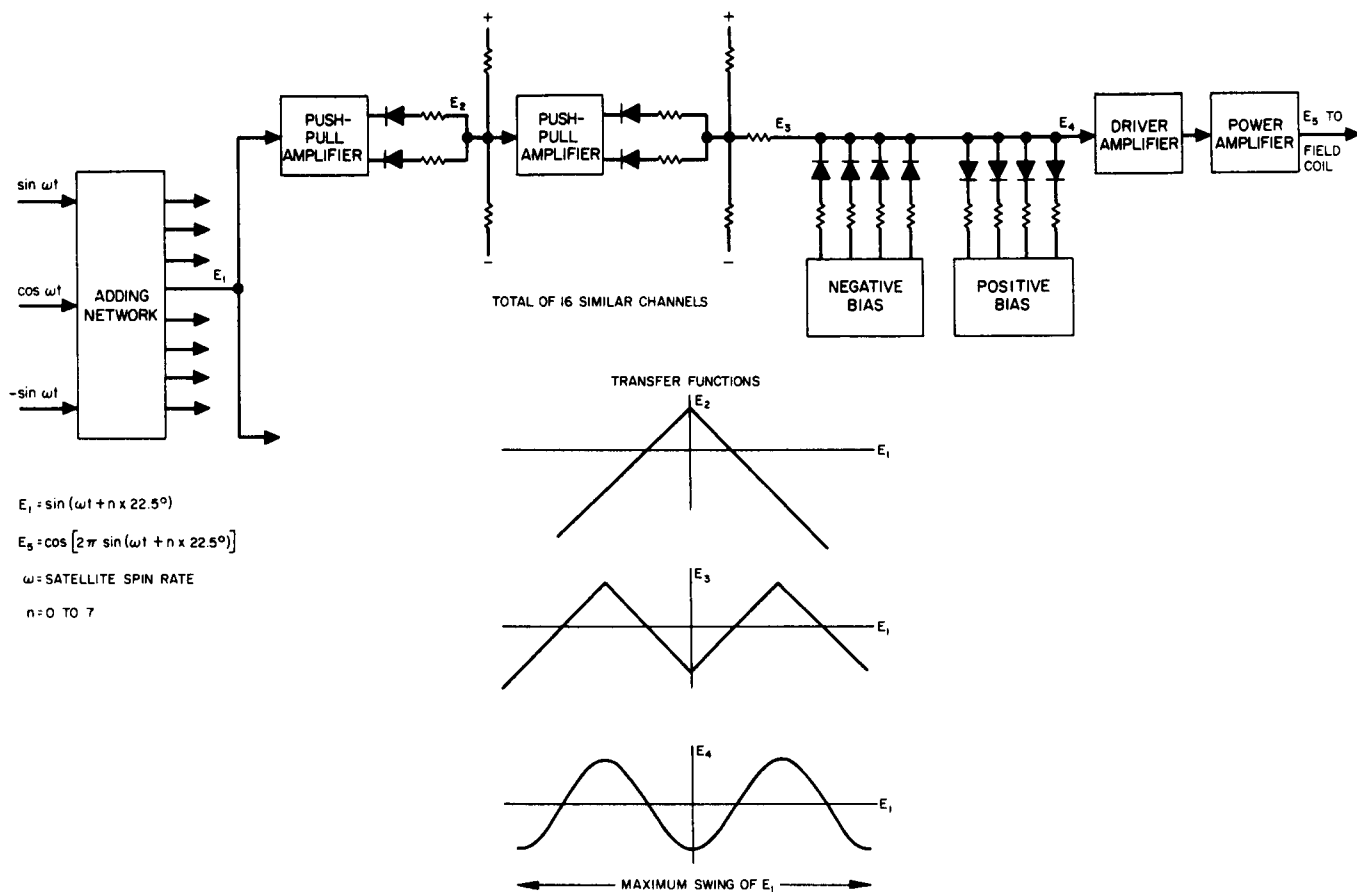
Figure 3-7. Major Functional Blocks of Analog Control
Electronics for Phased-Array Antenna
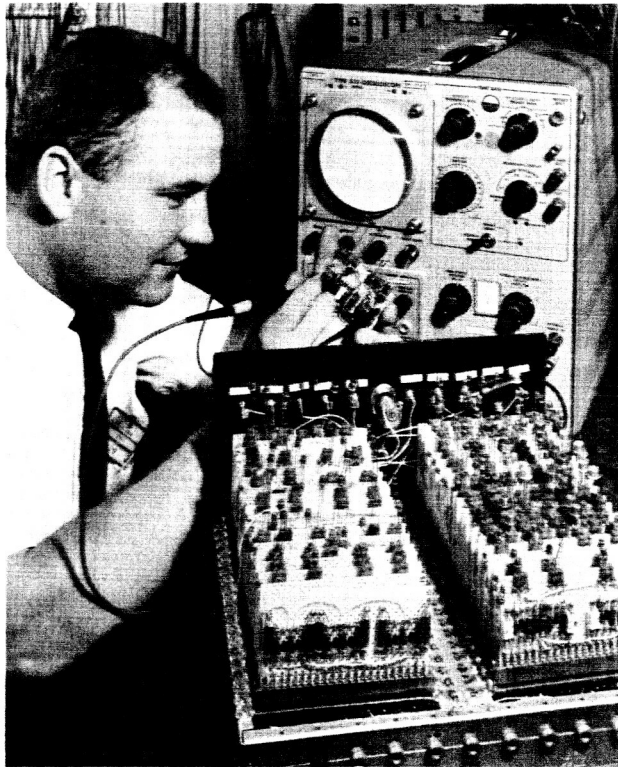
Figure 3-8. Circuit Checkout of Phase-Lock Loop Subassembly

Figure 3-9. Checkout of Phase-Lock
Loop Subassembly for Phased-Array
Antenna Digital Control Electronics
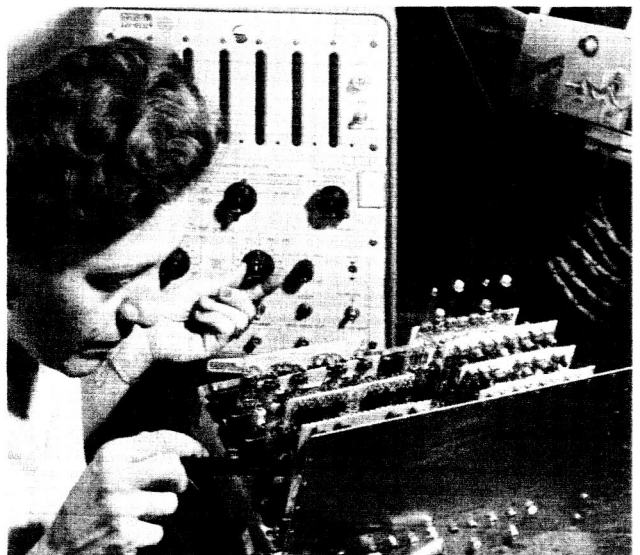
Figure 3-10. Electrical Checkout
and Test of Sine Wave
Generator Subassembly

Design of the units, which will be done early in December, has been greatly simplified by this choice of location.

Fabrication of the tester for the digital circuit cards was 80 percent complete on 1 December. Design of the digital unit tester was 50 percent complete.

A design review for the antenna control electronics is scheduled for mid-December.

Telemetry and Command Link for Phased-Array Antenna Demonstration

To demonstrate the capability of altering the direction of the antenna beam by command during the demonstration of the engineering model, RF telemetry and command link to the spinning spacecraft are required— telemetry, to indicate the direction of the beam and verify commands sent to the spacecraft, and command capability, to make any desired changes in the beam direction. Commands will also be used to demonstrate simulated pulsing of a hot gas jet. A light mounted on the surface of the spacecraft will be used to simulate the jet operation for these demonstrations.

The telemetry and command system will make use of existing equipment designs, including Mark I RF units. The command decoder and telemetry encoder will use Mark I telemetry and command simulator card designs for all but four cards.

Vertical Polarization

This antenna consists of a collinear array of basic dipole elements series-fed by coaxial-line slots. A bandwidth of 210 mc, centered at a frequency of 6300 mc, is required.

As previously reported, the use of "flared-skirt" dipole elements is being considered and the impedance properties of these elements are being investigated. The basic configuration of the element coupled to a series-fed air-filled coaxial line is shown in Figure 3-11.

For the preliminary set of data, the "flared-skirt" length is taken as a quarter-wavelength at center frequency. Two variable parameters are available, flare angle and spacing. A set of data was taken, yielding the results in Table 3-1 as recorded on the Smith Chart.

Analysis of this data disclosed that for a given spacing, the change in flare angle does not appreciably affect the admittance of the slot; but for a given flare angle, the change in spacing affects the values of conductance. This implies that fairly constant impedance characteristics can be achieved across the bandwidth required. For substantiation another set of data was taken. The results obtained are given in Table 3-2 as a function of frequency.

TABLE 3-1. ELEMENT IMPEDANCE CHARACTERISTICS

Flare Angle, degrees	Spacing			
	0.050 inch	0.100 inch	0.150 inch	0.200 inch
0	0.31-j1.81	0.60-j1.90	1.15-j2.15	2.00-j2.05
20	0.31-j1.80	0.62-j1.95	1.35-j2.30	2.20-j2.20
30	0.29-j1.76	0.62-j1.95	1.41-j2.30	2.15-j2.20
40	0.32-j1.74	0.76-j2.05	1.39-j2.15	2.30-j2.00

TABLE 3-2.
FREQUENCY SENSITIVITY
OF FLARED-SKIRT DIPOLE

Spacing = 0.200 inch,
Flare angle = 40 degrees

Frequency, mc	Impedance
5450	2.70-j1.10
5700	2.40-j1.50
5950	2.50-j1.90
6200	2.30-j2.00
6450	2.15-j2.10
6700	1.85-j1.90
6950	1.65-j1.70
7200	1.80-j1.90
7600	1.60-j1.60
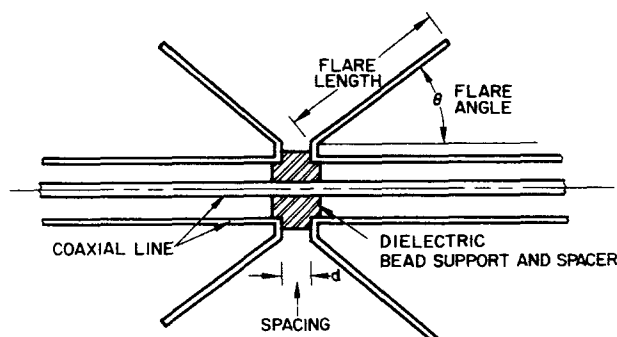
Figure 3-11. Flared Dipole
Radiating Element

This data indicates that the flared-skirted dipole definitely has impedance properties that vary slowly with changes in frequency. However, the large amount of reactance present indicates that the flare length is probably not correct. Variations in flare length will be investigated during the next report period. A computer run is being made to determine the effect of a reactive term on the pattern and gain.

A scaled version of the Syncom Mark I transmitting antenna was fabricated to operate at 6300 mc. Electrical measurements will begin the early part of the next report period.

Horizontal Polarization

The new symmetrical test section radiating element has been tested, with results indicating an omnidirectionality of less than 2 db. The final dimensions of the cloverleaf element have been determined and a six-element array is being fabricated. Several methods of matching the array over the required frequency band are being investigated.

During the next report period the following activities will be initiated:

1) Measurement of the input impedance of the six-element array over the frequency band;

2) Matching the impedance of the array over the frequency band;

3) Measurement of the radiation pattern of the array.

STRUCTURE

Structural Design

The majority (approximately 98 percent) of the structural drawings for the Engineering Shake Test Model, T-1, have been completed. The thrust tube spider assembly is composed of a 12-inch-diameter inner ring and 12 welded stiffeners (Figure 3-12). When assembled into the aft sub-assembly, the spider stiffeners will be riveted to the thrust tube stringers. The material for the solar panel attach fitting has been changed from magnesium to aluminum for increased stiffness. The forward and aft bulkheads have also been changed from magnesium to aluminum, and the aft bulkhead has been increased in gauge from 0.040 to 0.050. The aft ring has been decreased in gauge from 0.040 to 0.032, but has changed from magnesium to aluminum. The quadrant electronics package supports have also been changed from magnesium to aluminum. These changes are the result of the latest analyses of design loads.

During the next report period, the release of engineering drawings for structural test spacecraft T-1 will be completed. The T-1 will be an engineering model spacecraft reflecting the flight structural configuration. Units will be inert, dynamically similar, and as close to the final configuration in detail as possible. The purpose of the spacecraft test is twofold: 1) to confirm the dynamic properties of the spaceframe and to determine the effects on and measure the responses of the structure to random excitation; and 2) to confirm the structural capabilities of the spacecraft by subjecting the structure to a series of steady-state and vibratory loading conditions that
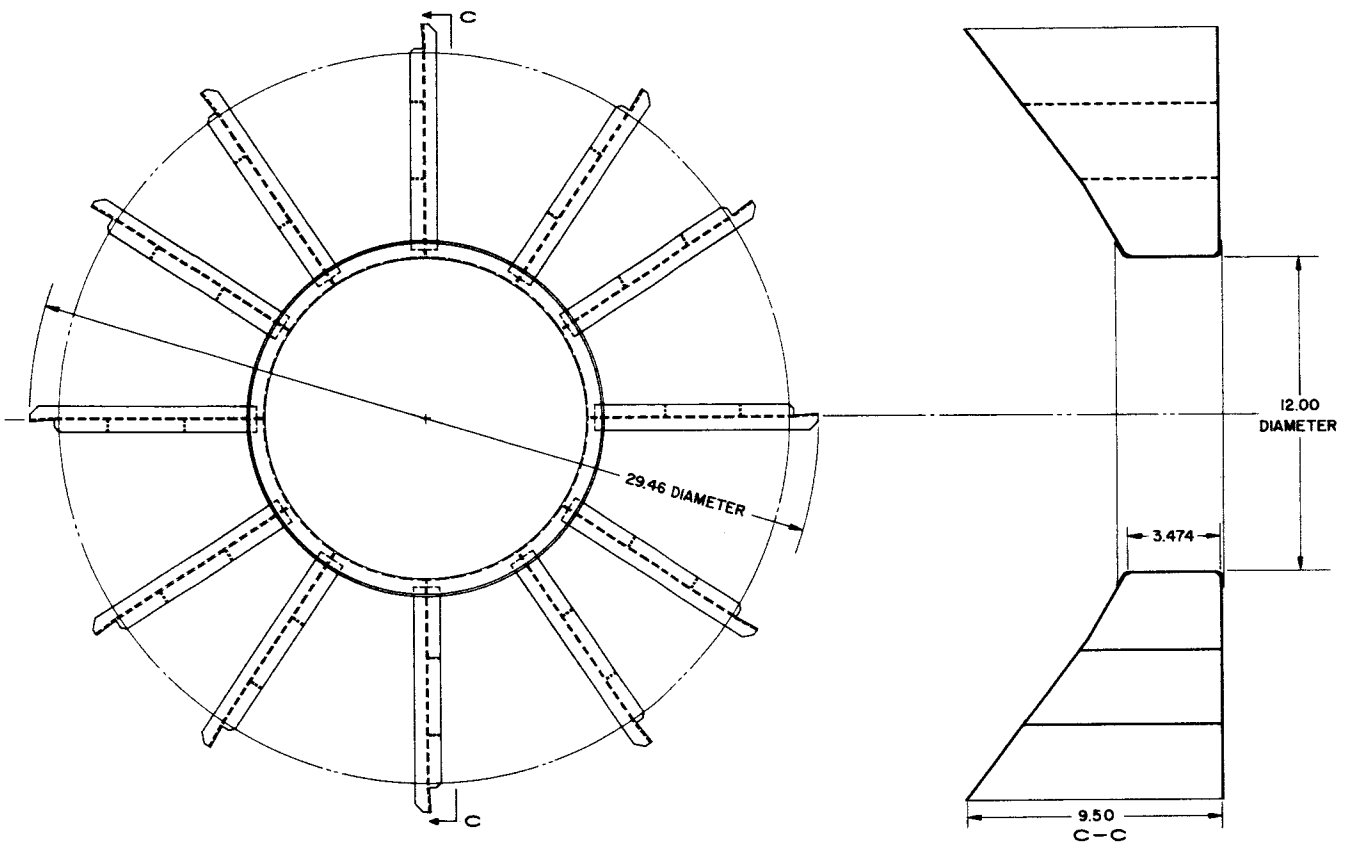
Figure 3-12. Thrust Tube Spider Assembly

will simulate the true load environment, i.e., the life cycle. The loads program has not yet been fully determined.

A full-scale wood and plastic mockup was completed during this report period (Figure 3-13).

Structural Analysis

A majority of the major subassemblies have been approved and released. The change in the forward and aft bulkheads from magnesium to aluminum was made for structural reasons, but it should also improve thermal properties. Two problem areas have been satisfactorily resolved analytically. One was the computed lack of torsional stiffness of the solar panel mountings. These supports have been stiffened considerably; however, testing will actually verify the structural adequacy. The other problem area was that of the electronic quadrant mountings. In this case dynamically suitable dummy electronic mountings will be incorporated in the test vehicle in such a way that test results can be obtained during the vibration testing for application to the final package design.

For dynamic analyses, an analytical model of ten degrees of freedom has been defined to obtain estimates of natural frequencies and unit responses. Calculation of stiffness coefficients for structural members has been initiated.

A vibration test plan for the engineering model is partially completed. Instrumentation of the engineering model will begin in the latter part of January 1963. This test will demonstrate the capability of the structure to withstand simulated launch environment levels, provide data for reducing structural weight, and provide qualification levels for components.

Weight Summary

Current weight data for the solid-propellant apogee motor configuration is summarized in Table 3-3. A detailed weight statement through final orbit condition is shown in Table 3-4.

Weight changes since the last weight statement are as follows:

Change	Weight, pounds
Antenna electronics support elimination	-1.2
Thrust tube length reduction	-1.4
Ring and bulkhead changes in material and/or gauges	+2.5
Solar panel attachment redesign	+1.3
Panel assembly bottle stiffening	+1.1
New hoist fittings	+1.5
Hardware and miscellaneous allocation for aft, center, and forward structure subassemblies	+3.9
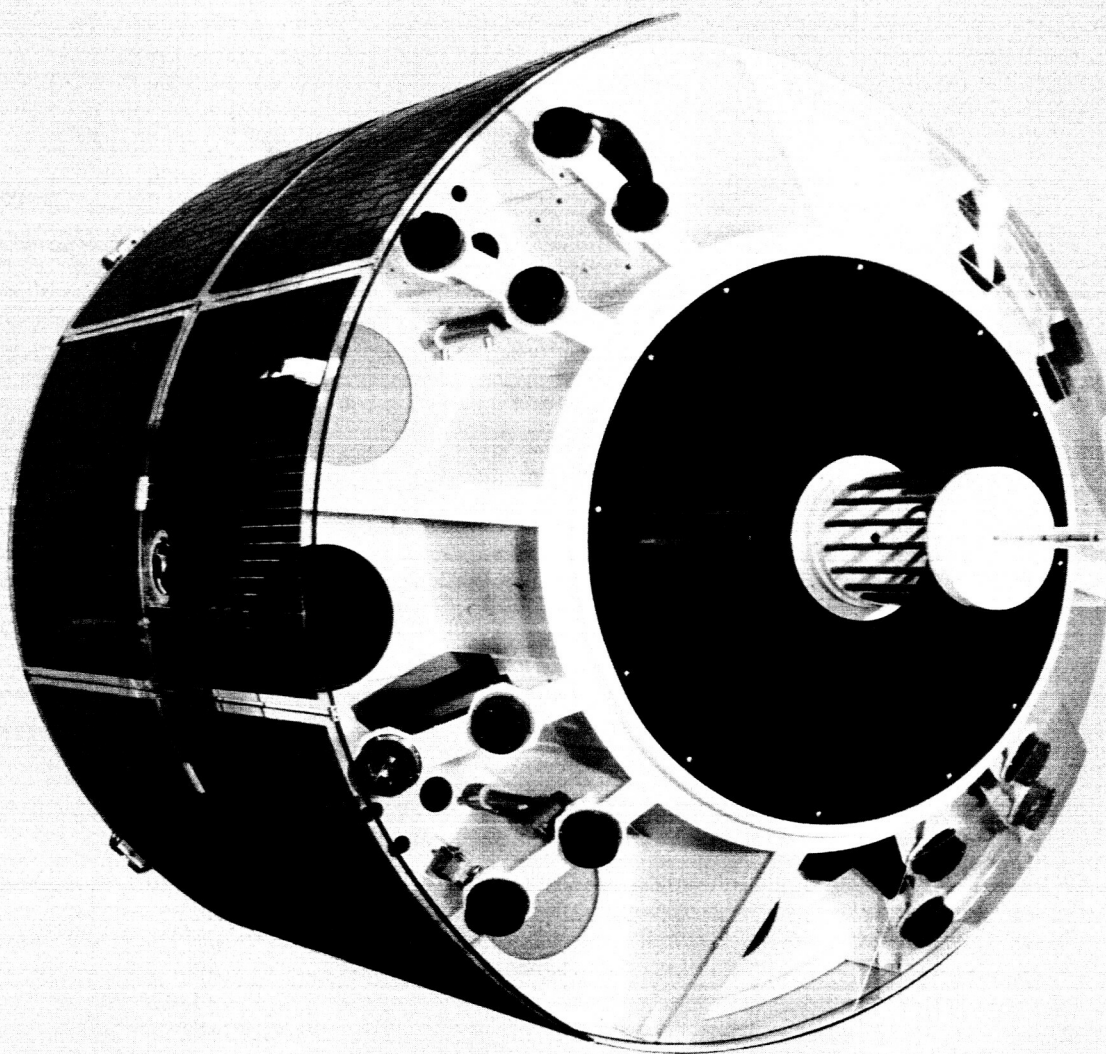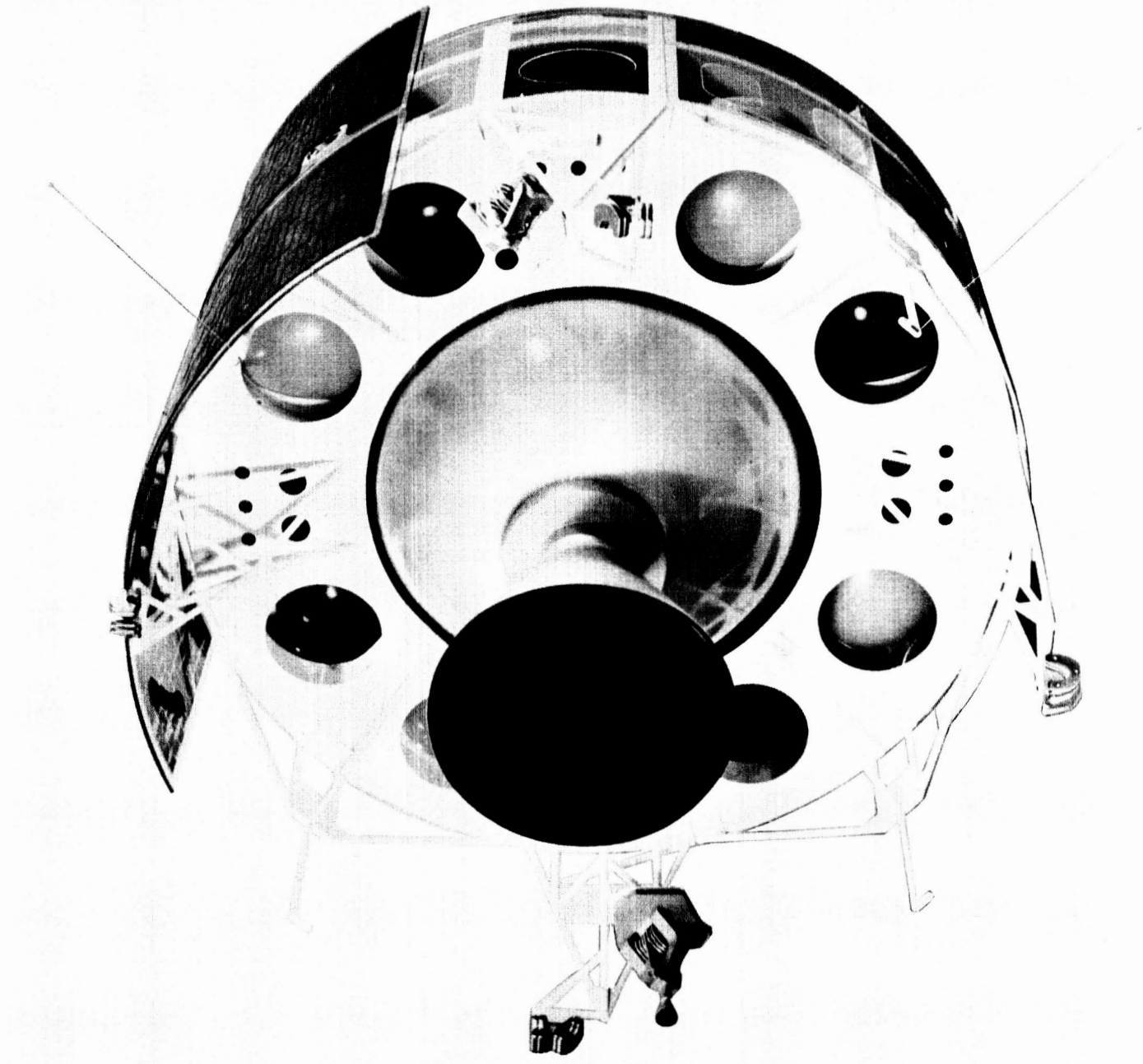
c) Forward View

b) Inboard Profile

a) Aft View
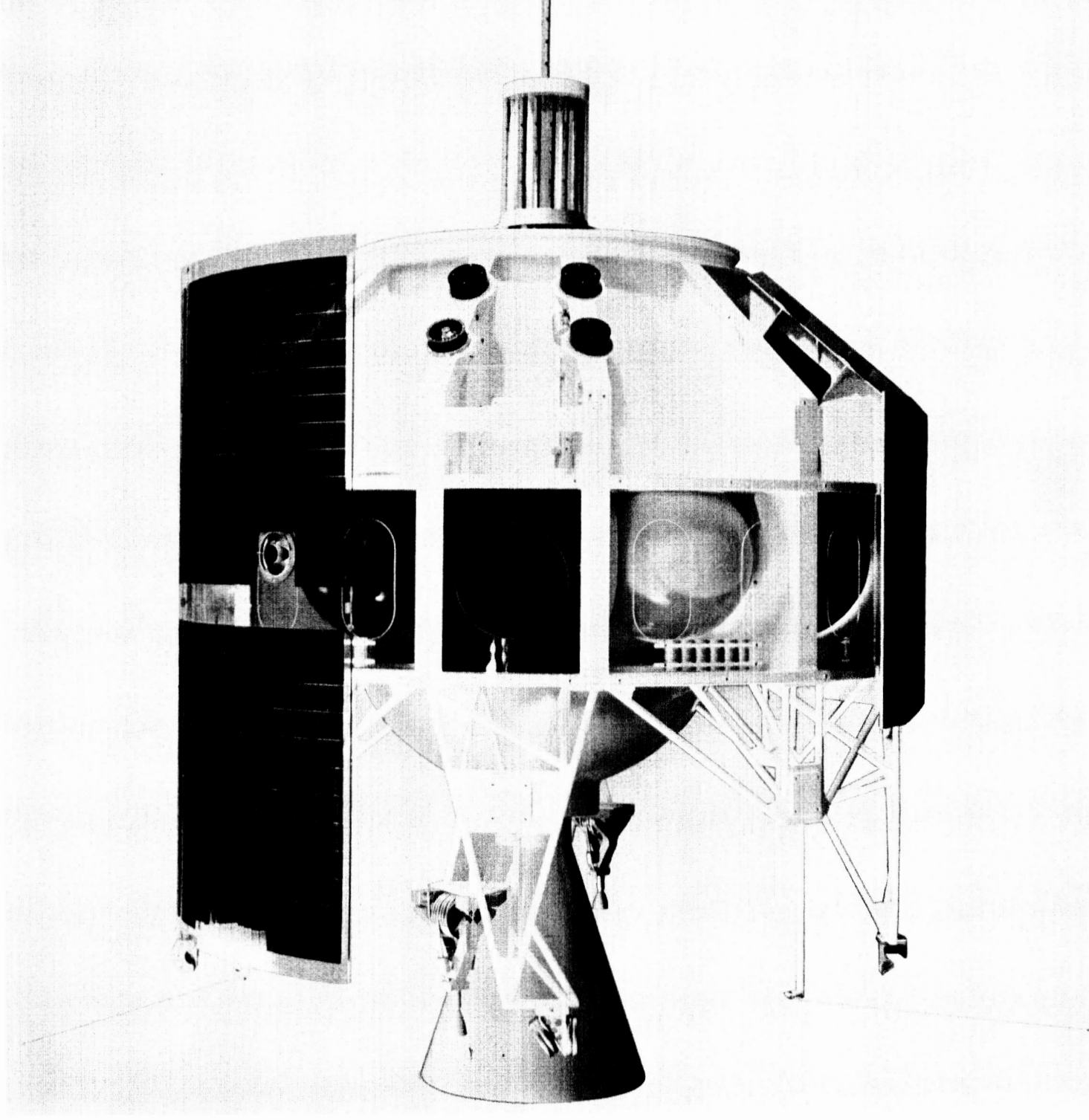
Figure 3-13. Syncom II Spacecraft Mockup Structure

TABLE 3-3. SYNCOM II ESTIMATED WEIGHT STATUS
Solid-Propellant Configuration

Subsystem	Δ Weight*	Weight, pounds	$\emptyset$**	θ***
Electronics		130.0	0.252	0.100
Wire harness		19.9	0.039	0.015
Power supply		102.6	0.199	0.079
Controls		38.6	0.075	0.030
Propulsion		75.1	0.145	0.058
Structure	+7.7	131.3	0.253	0.101
Miscellaneous		19.1	0.037	0.015

	Weight, pounds	Z-Z	I_{Z-Z}	I_{X-X}	R/P
Final orbit condition	(516.6)	23.5	53.6	41.0	1.31
N_2 pressurization	3.2				
N_2H_3-CH_3 fuel	55.6				
N_2O_4 oxidizer	92.4				
Total at apogee burnout	(667.8)	23.5	62.2	45.3	1.37
Apogee motor propellant	636.5				
Total payload at separation	(1304.3)	24.5	74.5	57.8	1.29

* = change in subsystem weight since last report.
** = ratio of subsystem weight to final orbit condition weight.
*** = ratio of subsystem weight to total payload at separation.

An expected decrease in weight due to spider assembly redesign will be made in the next report.

HANDLING, WEIGHT, AND BALANCE EQUIPMENT

During the period, design effort was directed toward the main assembly stand and associated structure assembly fixtures; the designs were completed and fabrication was initiated. Design of drill jigs, needed for drilling of holes in the forward and aft bulkheads, has begun.

TABLE 3-4. DETAILED WEIGHTS

Component	Δ Weight, pounds	Weight, pounds	
Electronic quadrants		80.00	
Telemetry transmitter		4.00	
Traveling-wave tube and converter		16.00	
Antenna electronics and supports		30.00	
Subtotal			130.00
Wire harness		19.90	
Subtotal			19.90
Battery packages		51.80	
Solar cells		22.80	
Solar cell supports		20.00	
Solar panel stiffeners		8.00	
Subtotal			102.60
Fuel and oxidizer tanks		13.00	
Thrust chambers		3.60	
Thrust chambers		2.60	
Fill and vent valves		1.20	
Spin control assemblies		2.50	
Spin control assemblies		2.50	

TABLE 3-4 (continued)

Component	ΔWeight, pounds	Weight, pounds	
Lines and fittings		2.00	
Miscellaneous		11.20	
Subtotal			38.60
Apogee motor installation		75.10	
Subtotal			75.10
Support antenna electronics	-1.20	-0.00	
Thrust tube		11.60	
Ring thrust tube	-1.40	4.90	
Ring stiffener		2.20	
Stringer tube		8.40	
Spider assembly		4.80	
Ribs		16.80	
Plate panel attachment	0.10	0.40	
Fitting panel attachment	1.20	2.20	
Ring, aft	-0.90	3.40	
Bulkhead, aft	3.20	6.60	
Hardware and miscellaneous	1.30	1.30	
Panel assembly, btl	1.10	25.10	
Ring, outer, large	-0.80	5.40	

TABLE 3-4 (continued)

Component	Δ Weight, pounds	Weight, pounds	
Ring, outer, small	-0. 20	1. 60	
Ring, inner	-1. 00	4. 60	
Support, electronics package 714	0. 20	1. 00	
Support, electronics package 715	0. 10	0. 40	
Hardware and miscellaneous 697	1. 30	1. 30	
Truss, jet		2. 70	
Truss, sun sensor		2. 30	
Truss, solar panel		4. 50	
Bulkhead, forward	2. 20	6. 00	
Tee, panel attachment	-0. 60	2. 40	
Support, electronics package	0. 20	1. 00	
Support, electronics package	0. 10	0. 40	
Hoist fitting	1. 50	1. 50	
Hardware and miscellaneous	1. 30	1. 30	
Hardware and miscellaneous		3. 90	
Battery supports	7. 70	3. 30	
Subtotal			131. 30
Paint		3. 00	
Thermal switch		4. 50	
Nutation damper		2. 00	
Miscellaneous		4. 60	
Dynamic balance adjustment		5. 00	
Subtotal			19. 10

TABLE 3-4 (continued)

	$\triangle$ Weight,* pounds	Weight, pounds	Z-Z	I_{Z-Z}	I_{X-X}	R/P
Final orbit condition	7.70	516.60	23.50	53.62	41.04	1.31
N_2 pressurization		3.20				
N_2H_3-CH_3 fuel		55.60				
N_2O_4 oxidizer		92.40				
Total at apogee burnout	7.70	667.80	23.50	62.18	45.32	1.37
Apogee motor propellant and expendables	7.30	636.50				
Payload at separation from booster	15.00	1304.30	24.50	74.47	37.84	1.29

Subsystem	Subsystem Weight to Final Orbit Condition Weight	Subsystem Weight to Total Payload at Separation Weight
Electronics	0.252	0.100
Wire harness	0.039	0.015
Power supply	0.199	0.079
Controls	0.075	0.030
Propulsion	0.145	0.058
Structure	0.254	0.101
Miscellaneous and balance adjustment	0.037	0.015

*$\triangle$Weight = change in subsystem weight since last report.

HOT GAS REACTION JET CONTROL SYSTEM

Propulsion Unit

Proposals for the development and delivery of a bipropellant reaction control system were received from seven of ten solicited bidders. All bidders proposed the use of monomethyl hydrazine as a fuel. Oxidizers proposed included MDFNA and various combinations of nitrogen tetroxide and nitrous oxide. There was a wide variation in the choice of valves and thrust chambers. The proposals are currently being evaluated. Source selection is expected to be made during the next report period.

Space Technology Laboratories declined to bid on the requested bipropellant system, but proposed a unit using hydrazine monopropellant. The STL proposal will be appraised with the bipropellant proposals.

Spin-Rate Control Mechanism

Design effort has been concentrated on the rotating jet scheme for spin-speed control. Detailed drawings of the basic mechanism will be completed by mid-December.

Design of the damper necessary to ensure the stability of the device is continuing.

Various forms of damping have been investigated including eddy-current, friction, and viscous. The eddy-current damper required to provide the necessary damping of 0.15 or greater, would weigh 10 pounds, considerably more than other dampers considered. Friction damping is obtainable by forcing a button of teflon against the spin control mechanism with a leaf spring. This is a simple scheme but the properties of teflon in ultra-low vacuums are not known well enough to allow the amount of friction to be controlled as closely as needed; too much friction is as undesirable as too little, since both can cause the mechanism to become insensitive, in varying degrees, to changes in spin-speed; i.e., a deadband is introduced. Since teflon is the subject of many space experiments, further consideration will be given the friction damper when additional pertinent properties are known.

A viscous damper with a bellows configuration appears to offer the required damping, reliability and low weight. The device shown schematically in Figure 3-14 consists of two bellows mounted on the spacecraft structure and joined by a plate attached to the fork of the spin control mechanism. An orifice in the plate allows fluid, (probably silicon) to pass from one bellows to the other. The length of the orifice will be large compared to the diameter to ensure laminar flow (in which the flow is proportional to pressure differential). Parts are being fabricated for the damper to allow verification testing. The test should be finished by the latter part of December.

Figure 3-14. Schematic Representation
of Viscous Damper

Design problems with the damper are due primarily to temperature effects and bulging of the bellows along its diameter. Expansion of the fluid can be accommodated by insertion of a small bellows at a position exactly between the two main bellows. This bellows will not affect the response or operation of the main bellows since the pressure at the midpoint is constant. Thus, it will serve only to accept the increased volume of fluid resulting from the temperature increase. The temperature environment of the damper will be from 0 to 110° F. The upper temperature is the result of a heat transfer analysis based on a conservative estimate of the maximum temperature existing at the base of the jet injection chamber (less than 200° F). The bulging of the bellows at the sides, an undesirable expansion, was found to affect the dynamic response of the bellows primarily in the same manner as an oil-spring. From preliminary tests already conducted, in which a single bellows was filled with water and subjected to compression, it was concluded that the effect of bulging was to contribute a spring gradient considerably weaker than the actual oil-spring gradient of the silicon fluid. The design must therefore compensate for this effect.

The brief analysis to follow indicates the nature of the effect of the bellows bulge (see Figure 3-14). Spring K_1 is the normal spring gradient associated with the bellows. It is shown distributed as four springs for reasons of symmetry. K_2 is the spring associated with the bulging of the bellows and is also shown distributed.

The mass of the fluid in bellows 1 is

$$m_1 = \rho V_1$$

where ρ is the density of the fluid and V is the volume.

3-27

Differentiating,

$$\dot{m}_1 = \rho \dot{V}_1 + V_1 \dot{\rho}$$

The flow, $Q_1 = \dfrac{\dot{m}_1}{\rho} = \dot{V}_1 + \dfrac{V_1}{\rho} \dot{\rho}$

The bulk modulus, $N = -V \dfrac{dP}{dv}\bigg|_{m=const.} = \rho \dfrac{dP}{d\rho}$

Substituting the above into the flow equation,

$$Q_1 = \dot{V}_1 + \dfrac{V_1}{N} \dot{P}_1$$

and similarly,

$$Q_2 = \dot{V}_2 + \dfrac{V_2}{N} \dot{P}_2$$

Since there is no leakage and the bulk modulus is constant it is possible to write

$$\dot{P}_1 = \dfrac{-V_2}{V_1 + V_2} \dot{P}_L \text{ and } \dot{P}_2 = \dfrac{V_1}{V_1 + V_2} \dot{P}_L$$

where $P_L = P_2 - P_1$.

Substituting into the flow equation,

$$Q = \dot{V} - \dfrac{V_e}{N} \dot{P}_L \text{ where } V_e = \dfrac{V_1 V_2}{V_1 + V_2}$$

The orifice will be designed to produce laminar flow, i.e.,

$$Q = C P_L$$

where C is the orifice coefficient.

Equating the equation for Q and recognizing that $\dot{V} = a\delta$, where a is the area

of the plate between the bellows and $\dot{\delta}$ the velocity of the plate, P_L can be related to the displacement δ in LaPlace transform notation as,

$$\frac{P_L}{\delta} = \frac{a/c \ S}{\frac{V_e}{NC} S + 1}$$

The forces acting in the bellows plate are

$$F = aP_L + K_1 \delta$$

Substituting for P_L, the transfer function of the damper is,

$$\frac{F}{\delta} = \frac{\frac{a^2}{c} S}{\frac{a^2}{CK_2} S + 1} + K_1$$

K_2 is the oil-spring of the fluid due to its compressibility and can be shown to equal $\frac{a^2 N}{V_e}$. The spring associated with the bulging of the bellows acts in exactly the same manner; i. e. , in the case in which the orifice is blocked, the center plate is able to move when a force is applied, due to either oil compression or bellows bulging or both. The oil-spring is considerably stiffer than that associated with bulging; therefore, K_2 will be considered to be the "bulging" spring. The term $\frac{a^2}{c}$ in the equation in the damping evident when K_1 is zero and K_2 is infinite.

The effect of the lag term is to cause the damper to act like a spring for frequencies above the lag breakpoint. To ensure that damping is provided near the natural frequency of the spin-control mechanism the lag breakpoint should be at least several times the natural frequency. The bellows spring K_1 should be small relative to the primary spring of the spin-control mechanism (the bipropellant tubes). Knowing K_1 and the desired minimum damping, it is necessary to so choose a bellows that K_2 , the "bulging" spring is large enough to meet the lag breakpoint requirement.

During the month of December, design of the spin control mechanism will continue. The detail drawings for the basic spin control mechanism will be completed and fabrication of parts started. The damper configuration will be selected and tested.

4. STUDIES OF ALTERNATE CONFIGURATIONS

SYSTEM STUDIES

A study was conducted to evaluate the feasibility of using the Allegany Ballistics Laboratory engine ABL-248 as an apogee engine for Syncom II. The study consisted of a weight and balance analysis and a structural layout.

The approach taken in the weight analysis was to consider a scaled-down Syncom II that could be injected into the synchronous orbit. The weight breakdown is shown in Table 4-1. The ratio of major subsystems are shown in Table 4-2. Only two electronic quadrants are included and only two telemetry transmitters. As a consequence, the control subsystem was scaled to contain only two fuel and oxidizer tanks.

The weights for the ABL-248 engine were taken from Allegany Ballistics Laboratory reports and are to be considered typical of these engines. For the purposes of the analysis, the engine was considered to be in a fully loaded condition. Although the final orbit payload weight resulting was not the optimum that could be achieved with the ABL-248 engine, the weight of 379.4 pounds provides an indication of the engine's capability.

Table 4-3 illustrates weight and balance status at various times in the trajectory. The table shows that the roll-to-pitch moment of inertia at payload separation from the booster does not meet the design objective of 1.2. At apogee motor burnout, however, this value approximates the desired design objective. In the final orbit condition, after expulsion of the control system liquids, the ratio again is unacceptable.

Several methods can be employed to relieve these deficiencies. First, the amount of propellant could be reduced (which was not considered in this study, in which a fully loaded condition was used). Secondly, the engine could be moved aft of the location shown in Figure 4-1. Thirdly, a rearrangement of the internal equipment would place more weight closer to the outer diameter.

In the post-apogee motor burnout and final orbit conditions, it is quite possible to achieve higher roll-to-pitch moment of inertia ratios. However, the condition at separation from the booster appears to be difficult to improve adequately.

TABLE 4-1.   WEIGHT BREAKDOWN OF A SCALED-DOWN MARK II

Item	Weight, pounds	
Electronic quadrants, 2	50.00	
Telemetry transmitter, 2	2.00	
TWT, 4	4.00	
DC converters, 4	4.00	
Relay, filter, and coupler, 2 each	1.50	
Antenna electronics	30.00	
Whip antenna, 4	0.20	
Subtotal		91.70
Wire harness	10.00	
Subtotal		10.00
Battery packages	51.80	
Solar panels	42.80	
Subtotal		94.60
Fuel tanks, 2	3.25	
Oxidizer tanks, 2	3.25	
Miscellaneous	5.60	
Thrust chamber	1.30	
Thrust chamber	1.80	
Spin control assembly	1.30	
Spin control assembly	1.30	
Valves, lines, and fittings	1.60	
Subtotal		19.40
Apogee motor	42.60	
Apogee motor hardware	1.00	
Subtotal		43.60

TABLE 4-1 (continued)

Item	Weight, pounds	
Thrust tube, 063 aluminum	20.20	
Ring thrust tube, aluminum	6.00	
Ring stiffener, aluminum	1.00	
Spider assembly, magnesium	6.00	
Truss, aluminum	10.00	
Bulkhead, 05 magnesium	7.00	
Outer ring, 063 magnesium	11.40	
Panel mounting, magnesium, 8	18.00	
Tee stiffener, 063 aluminum, 8	5.00	
Tee magnesium, 8	1.50	
Panel attachment, aluminum	3.00	
Channel 093, aluminum	6.70	
Battery supports	3.30	
Hoist fittings	2.00	
Hardware plus miscellaneous	4.00	
Subtotal		105.10
Paint	3.00	
Nutation damper, 2	2.00	
Miscellaneous equipment	5.00	
Dynamic balance	5.00	
Subtotal		15.00

TABLE 4-2. RATIO OF SUBSYSTEM WEIGHTS TO FINAL ORBIT
WEIGHT AND TO SEPARATION WEIGHT

Subsystem	Subsystem Weight to Final Orbit Condition Weight	Subsystem Weight to Total Payload at Separation Weight
Electronics	0.242	0.100
Wire harness	0.026	0.011
Power supply	0.249	0.103
Controls	0.051	0.021
Propulsion	0.115	0.114
Structure	0.277	0.114
Miscellaneous and balance	0.040	0.016

TABLE 4-3. WEIGHT AND BALANCE STATUS FOR TWO
POINTS IN TRAJECTORY

	Weight, pounds	Z-Z	I_{Z-Z}	I_{X-X}	R/P
Final orbit condition	379.40	22.00	35.09	36.75	0.95
N_2 pressurization	1.60				
N_2H_3-CH_3 fuel	27.80				
N_2O_4 oxidizer	46.20				
Total at apogee burnout	455.00	22.00	42.12	37.95	1.11
Apogee motor propellant plus inerts	464.40				
Payload at separation from booster	919.40	30.08	45.77	65.97	0.69

LAYOUT OF SYNCOM/ABL-248 CONFIGURATION

Figure 4-1 illustrates a possible layout of the ABL-248 engine within a modified Syncom II vehicle. Some of the significant changes in the Syncom II were:

1) Reduction of the number of electronic quadrants from four to two.

2) Reduction of control system tanks from eight to four.
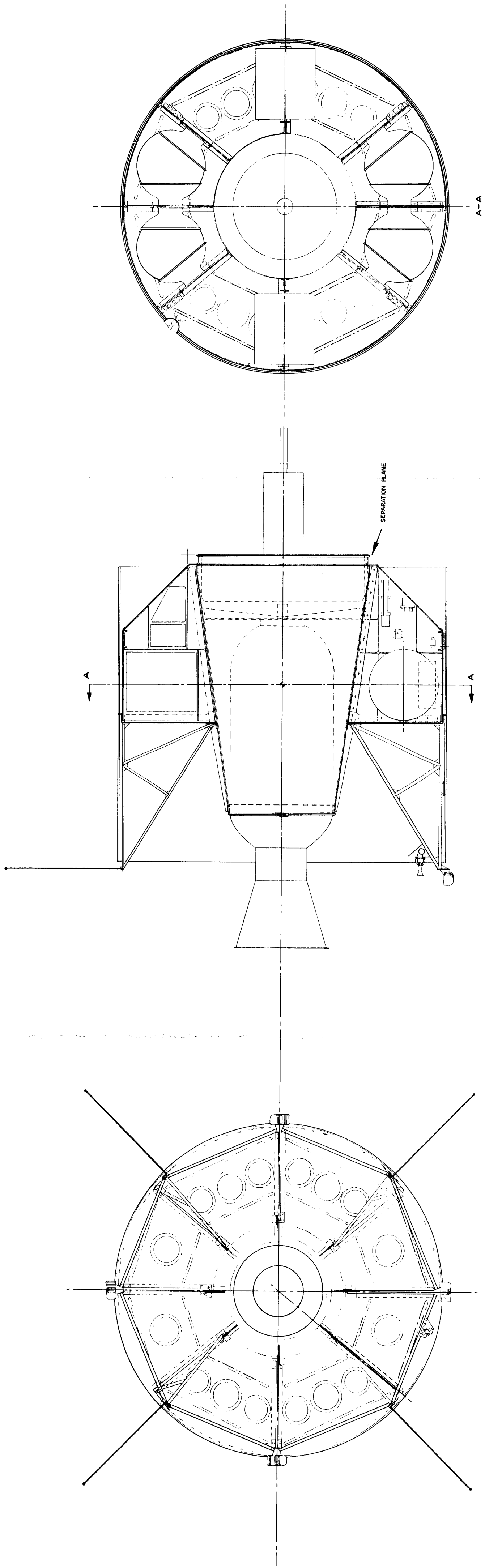
3) Scaling down of the structural subsystem.

Figure 4-1. ABL-248 Engine Layout

SEPARATION PLANE

A—A

A   A

4-5

As shown above, this configuration has an unsatisfactory roll-to-pitch moment of inertia.

The alternate spacecraft structure utilizing the ABL-248 apogee motor consists of a conical aluminum thrust tube built up from sheet metal and machined parts. A machined ring provides the interface for the Atlas-Agena. Another machined ring mates with the ring on the ABL-248 apogee motor at the nozzle end and is fastened to the motor by means of a Marman clamp. These two rings are riveted to a cone-shaped tube of sheet metal with eight exterior tee stiffeners running fore and aft. These stiffeners provide the surfaces to which the control jet fuel tank mounting panels and quadrant electronic package mounting panels are riveted. The mounting panels are machined from magnesium plate with integral stiffening ribs and provide surfaces for mounting four control jet fuel tanks, two quadrant electronic packages and four storage battery packages. The aft end of the apogee motor is attached to a spider-like stiffener machined from magnesium and riveted to the thrust-tube assembly.

Both the bulkhead and outer ring are fabricated from sheet magnesium employing lightening holes and beads for added stiffness. Aluminum sheet metal channels separate the mounting panels at their aftmost outer edges. The connection between the bulkhead and mounting panels is made with the use of a magnesium tee riveted to the bulkhead and bolted to the mounting panels.

The individual truss work towers supporting the four sun sensors, single orientation jet, and four telemetry and command whip antennas are fabricated from round aluminum tubing and sheet metal gussets welded in place and attached as separate units to the bulkhead by bolts.

The 16 solar cell panels are fabricated and mounted in a manner similar to that of the current solid apogee motor configuration, providing center mounting. The two quadrant electronic packages are attached to mounting panels 180 degrees apart. Each of these packages is split and mounted on both sides of the panel. Mounting of the control jet fuel tanks and the single velocity jet is similar to that of the current configuration. Four of the six tank mounting panels are also used for mounting four storage battery packages, four traveling-wave tubes, and four dc converters. Two mounting panels each carry a telemetry transmitter.

RECOMMENDATIONS

The Hughes study of an ABL-248 engine for apogee boost found it to be unsatisfactory for the particular design parameters. Its roll-to-pitch moment of inertia did not meet Syncom design objectives. Some variation in the design could increase this ratio; the large pitch-to-roll ratio of the loaded motor itself, however, would be extremely difficult to overcome.

4-7

5. NEW TECHNOLOGY

PROBABILISTIC MODEL FOR SPACECRAFT AVAILABILITY AND REPLACEMENT RATE

Probabilistic models for spacecraft availability and replacement rate have been developed and in this section a summary of the steps in the mathematical development is presented.

The probability of a spacecraft failure prior to, during, and after replacement are characterized by three failure modes (Figure 5-1). Formulation of the utilization, outage, and duplication times yields equations that describe the function of useful time (up-time ratio or availability), fractions of nonuseful time (down-time ratio), and fraction of duplication time. Mathematical models for the number of satellites needed and replacement rate are presented. Numerical estimates of availability and replacement rate for one spacecraft based upon the probability of survival of at least one of four communications quadrants (Figure 5-2) illustrates the models.

System Description and Definitions

In this system, a communication satellite has a known distribution of life times given in Figure 5-1. A single satellite is in operation. Some replacement rule (to be discussed in a succeeding paper) is used to establish r, the time of decision to replace the satellite. At time S later, the satellite is replaced. The replacer has perfect and instantaneous knowledge of satellite's status (live or dead).

Three failure modes can be described:

Mode 1: The satellite fails at time j, before the replacement decision is made, the replacement decision is instantly made, and replacement occurs at time S later, i.e., at time j + S.

Mode 2: The satellite lives until time r but fails between r and r + S, i.e., after the replacement decision is made, but before the replacement is completed. Failure occurs at r + k.
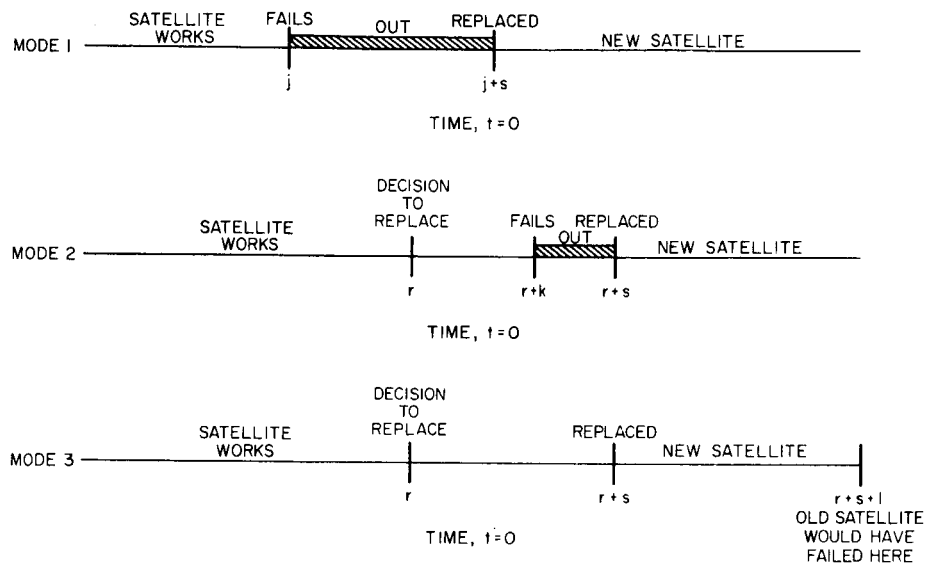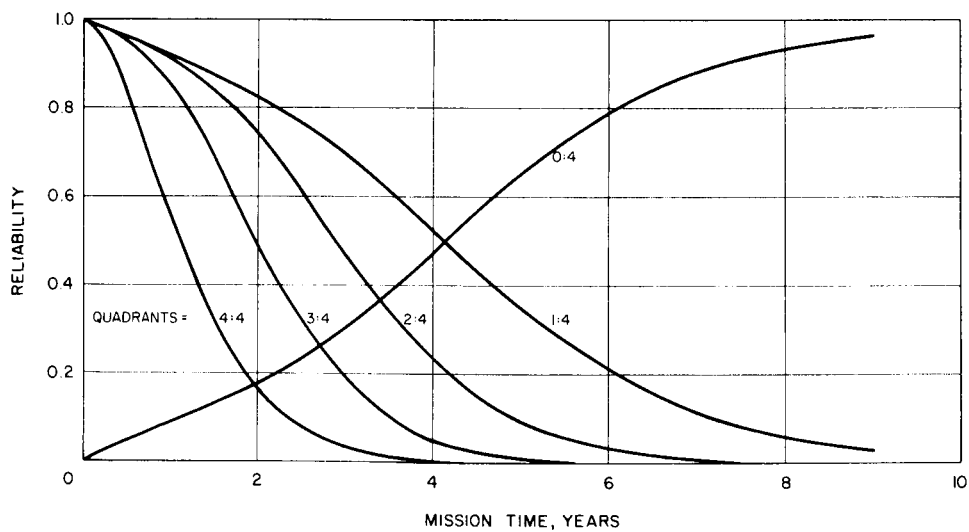
Figure 5-1. Spacecraft Failure Modes

Figure 5-2. Quadrant Probability of Survival,
Multiple-Access Communications Mode

5-2

Mode 3: The satellite lives until time r and then until after r + S; i.e., after replacement has been completed the original satellite is still in working order. Furthermore, the original satellite is removed, even though still usable, as soon as replacement is complete. If it were not removed, it would fail at some later time r + S + 1. Figure 5-1 illustrates the three failure modes and aids in the definition of the terms.

The probability of failure by time t will be indicated by P(t). Thus,

$P(r)$ = probability of satellite failure between time zero and time r, which is the time of decision to replace

$P(r + S)$ = probability of failure by time r + S, etc.

Utilization, Outage, and Duplication Times

Consider a period of time T long enough to be essentially infinite compared to any single satellite lifetime. It will be composed of a random mixture of satellite lifetimes, each ending in one of the three failure modes.

The length of time due to each Mode 1 failure will be j + S, and of this j will be useful and S will be nonuseful. N will be the total number of satellites used in time T. The probability of failure in Mode 1 will be P(r). Therefore, the expected time spent by satellites that fail in Mode 1 will be:

$$N \left[P(r)(j + S) \right] \qquad \text{total time}$$

$$N \left[P(r)(j) \right] \qquad \text{total useful time (live satellite)}$$

$$N \left[P(r)(S) \right] \qquad \text{total nonuseful time (dead satellite)}$$

The length of time due to each Mode 2 failure will be r + S, and of this r + k will be useful and S - k will be nonuseful time. The probability of failure in Mode 2 will be P(r + S) - P(r), that is, the probability of failing by time r + S minus the probability of failing by time r. Therefore, the expected times spent by satellites that fail in Mode 2 will be:

$$N \left[P(r + S) - P(r) \right] (r + S) \quad \text{total time} \qquad (5-1)$$

$$N \left[P(r + S) - P(r) \right] (r + k) \quad \text{total useful time (live satellite)} \qquad (5-2)$$

$$N \left[P(r + S) - P(r) \right] (S - k) \quad \text{total nonuseful time (dead satellite)} \qquad (5-3)$$

The length of time due to each Mode 3 failure will be r + S and will be all useful. The length of time that would be spent by the old satellite after replacement as duplication time if it were not removed at replacement is 1. The probability of failure in Mode 3 will be 1 - P(r + S). Therefore, the expected times spent by satellites that fail in Mode 3 will be:

$$N \left[1 - P(r + S)\right] (r + S) \qquad \text{total time} \qquad\qquad (5\text{-}4)$$

$$N \left[1 - P(r + S)\right] (r + S) \qquad \begin{array}{l}\text{total useful time}\\ \text{(live satellite)}\end{array} \qquad (5\text{-}5)$$

$$N \left[1 - P(r + S)\right] (1) \qquad \text{total duplication time} \qquad (5\text{-}6)$$

These expressions can be combined in various ways:

$$T = N \left\{ P(r)\,(j + S) + \left[P(r+S)\ P(r)\right](r+S) + \left[1 - P(r+S)\right](r+S) \right\} \quad (5\text{-}7)$$

$$= N \left\{ (j - r)\,P(r) + (r + S) \right\} \qquad\qquad (5\text{-}8)$$

$$T_{useful} = N \left\{ P(r)(j) + \left[P(r+S) - P(r)\right](r+k) + \left[1 - P(r+S)\right](r+S) \right\} \quad (5\text{-}9)$$

$$= N \left\{ P(r)(j - r - k) + P(r+S)(k - S) + (r + S) \right\} \qquad (5\text{-}10)$$

$$T_{nonuseful} = N \left\{ P(r)(S) + \left[P(r+S) - P(r)\right](S - k) \right\} \qquad (5\text{-}11)$$

$$= N \left\{ k\,P(r) + (S - k)\,P(r + S) \right\} \qquad (5\text{-}12)$$

$$T_{duplication} = N \left[1 - P(r + S)\right](1) \qquad (5\text{-}13)$$

Fraction of nonuseful time is:

$$\frac{T_{nonuseful}}{T} = \frac{k\,P(r) + (S - k)\,P(r + S)}{(j - r)\,P(r) + r + S} \qquad (5\text{-}14)$$

Fraction of useful time is:

$$\frac{T_{useful}}{T} = \frac{(j - r - k)\,P(r) + (k - S)\,P(r + S) + (r + S)}{(j - r)\,P(r) + (r + S)} \qquad (5\text{-}15)$$

Fraction of duplication time is:

$$\frac{T_{duplication}}{T} = \frac{(1)\left[1 - P(r + S)\right]}{(j - r)\,P(r) + (r + S)} \qquad (5\text{-}16)$$

Numbers of Satellites Needed

The number of satellites needed in time T will be designated N, and T = N L, where L is the mean satellite useful life. Since there are three failure modes, this can be broken down into N_1, N_2, and N_3, with L_1, L_2, and L_3 for mean lives. Then

$$N = N_1 + N_2 + N_3 \qquad (5\text{-}17)$$

$$T = T_1 + T_2 + T_3 \qquad\qquad (5\text{-}18)$$

and so

$$T = N_1 L_1 + N_2 L_2 + N_3 L_3 \qquad\qquad (5\text{-}19)$$

and

$$N = \frac{T_1}{L_1} + \frac{T_2}{L_2} + \frac{T_3}{L_3} \qquad\qquad (5\text{-}20)$$

The rate of replacement of satellites is given by

$$\frac{N}{T} = \frac{1}{L} = \frac{1}{(j - r)\, P(r) + (r + S)} \qquad\qquad (5\text{-}21)$$

Numerical Values

The lifetime characteristic for Syncom II given in Figure 5-2 enables estimation of the fraction of useful time and the expected launch rate. If a satellite is replaced on the average of every 2 years, unless a failure occurs sooner, the $r = Z$. Because of the knowledge of the satellite status, this does not mean an arbitrary replacement at 2 years, but rather a replacement based on some stated criterion that occurs on the average of every 2 years, such as having at least three channels functioning. The rest of the parameters are as follows as determined from Figure 5-2.

$$r = 2 \text{ years}$$

$$P(r) = 0.18$$

$$S = 0.2 \text{ year}^{*}$$

$$j = 1 \text{ year}$$

$$k = 0.1 \text{ year}^{*}$$

$$P(r + S) = 0.20$$

---

*Reaction time is 0.1 year, but because of boost failures 50 percent of the time S must be increased to 0.2 year and k to 0.1 from 0.05.

For convenient numerical evaluating

$$\frac{T_{useful}}{T} = 1 - \frac{T_{nonuseful}}{T} \qquad (5-22)$$

substituting

$$\frac{T_{useful}}{T} = 1 - \frac{k(Pr) + (S-k) P (r+S)}{(j-r) P (r) + r + S}$$

$$= 0.9812$$

The number of satellites needed is evaluated from Equation 5-21 using the same parameters.

$$\frac{N}{T} = \frac{1}{2.02} = 0.495 \text{ per year}$$

The replacement rate is equal to N/T divided by the boost reliability 0.5 or 0.99 per year.

These conclusions are conservative in that possible use of satellite communication channels in those satellites which had called for replacement is neglected.

It is interesting to compare this result with that for a satellite with the lifetime characteristics of Syncom II, which is replaced only upon complete failure. Maintainability theory gives

$$\frac{T_{useful}}{T} = \frac{1}{1 + \frac{S}{\lambda}} \qquad (5-23)$$

When S is as before the replacement time and λ is the mean life for at least one channel (4 years)

$$\frac{T_{useful}}{T} = \frac{1}{1 + \frac{0.2}{4}} = 0.952$$

5-6

Cost effectiveness considerations make use of this model in order to optimize the decision criteria adopted for Syncom II.

The above analytical techniques are considered by the contractor to be unique, but are not considered an invention, per se.

The analytical techniques described provide tools required in the system reliability analyses. The degrees of subsystem redundancy and system criteria for satellite replacement are important parameters, the determination of which is aided by the techniques described.

The analytical techniques may be applied to satellite replacement criteria wherein system redundancy and a minimum continuous capability are complicating requirements.

6. PROJECT REFERENCE REPORTS

- J. M. Zajec, "Trip Report " - Attendance at Project Telstar Component Reliability Symposium, Murray Hill, New Jersey, 14 November 1962. Report dated 20 November 1962.

- M. J. Neufeld, "Bendix Photo-Detector for Syncom Attitude Reference," Technical Report, 27 November 1962 (See Appendix A).

- Paul M. Blair, Jr. and Herbert Y. Tada, "Environments of Syncom Mark II," TM 732, October 1962.

APPENDIX A. BENDIX PHOTODETECTOR FOR
SYNCOM ATTITUDE REFERENCE

A preliminary examination of the physical properties of a miniature photodetector and a nonmechanical scanning system described in Reference A-1 is made to show its feasibility as a body-mounted detector of the star Polaris and hence as a more precise attitude reference for Syncom. It is assumed that the existing Syncom attitude reference and control system will bring the spacecraft spin axis to within 2.5 degrees of the line of sight to Polaris, i.e., half the field of view of the detector.

A simplified, single-channel, PPI type scanning method with angle referenced to the sun sensor pips may be more suitable than the two-channel linear raster scan indicated in Reference A-1, since the rotation of the satellite about its spin axis naturally provides the angular sweep motion of a polar coordinate system. In either case, however, some degradation of spin angle resolution results for star images near the center of the field due to overlap of the scanning line which is 0.5 degree wide. A linear raster scan outlined by Bendix does not preclude this difficulty, although some extra electronics will be needed to despin the rotating field of view.

Optics of 1.5 inches diameter and a video bandwidth of about 10 kc should provide adequate signal-to-noise ratio $\geq$ 2 at the input to a video amplifier with a resolution of 15 minutes of arc when aimed at Polaris. The attitude control precision, however, will be limited by the available spin angle resolution, $\left(\dfrac{360 \text{ degrees}}{512} \approx 0.7 \text{ degree} \right)$ plus sun sensor errors (~ 0.2 degree). The direction of the angular difference (~ 0.9 degree) between the earth's polar axis and the line of sight to Polaris can be determined from knowledge of Polaris mean right ascension and the sun ephemerides at the satellite longitude. In addition, the telemetered video information of the field of view (e.g., in the form of a video display on a multimode storage tube referenced to the satellite-sun line) can be used to readily discriminate against fainter stars appearing in the 5-degree field, (e.g., δ -Ursa Minor), by visual inspection, by using some suitably prepared star-field mask, or automatically.

A solid-state (no moving parts) phototropic screen is proposed as an alternate to a mechanical shutter to protect the photocathode from possible damage due to sun imaging during the initial ascent and orientation sequence.

The phototropic screen is claimed to go from a transparent to an opaque state within a few microseconds after exposure to strong ultraviolet light. Transparency is regained in a few seconds after removal of the ultraviolet light.

BENDIX PHOTODETECTOR, ELECTRON MULTIPLIER, AND PROPOSED TRACKER (REFERENCE A-1)

The Bendix channel photomultiplier (photodetector and electron multiplier) weighs 1.2 ounces, occupies 2.5 cubic inches, and has provisions for image scanning. Bendix proposes to build a tracker (using coarse and fine scans) with this tube with the specifications listed in Table A-1.

TABLE A-1. PROPOSED BENDIX TRACKER SPECIFICATIONS

Weight:	3 pounds
Volume:	95 cubic inches
Power:	5 watts (1 to 2 kilovolts at 2×10^{-7} ampere needed for channel multiplier)
Field of view:	5 degrees total 0.5 degree instantaneous (coarse scan) with 50 percent overlap
Pointing accuracy:	
Coarse scan:	±0.25 degree (linear raster scan, saturated output)
Fine scan:	±9 seconds of arc (cross scan, proportional output, when viewing third magnitude stars or brighter)
Output saturation level:	±6 volts (15 minutes of arc error)
Sensitivity:	0.4 volt per minute of arc to saturation
Linearity:	10 percent over 30 minutes of arc
Sampling rate:	25 frames per second
Photocathode characteristic:	S-11 (see text)

Photodetector

When an image of a star falls on the photocathode, the electron stream emitted at that spot is focused to a fine bundle in the plane of the aperture by means of the electrostatic lens (Figure A-1). Should the electron stream enter the aperture, it undergoes a process of amplification by the electron multiplier shown schematically.

In general, owing to pointing error, the image will not fall exactly on the optical axis but will be displaced some radial distance r and angle θ (with respect to a reference) on the cathode. For this case the electron stream would miss the aperture and the output of the electron multiplier would be zero. However, the magnetic deflecting scanning fields applied to the region behind the cathode are such that an off-axis electron stream is eventually introduced into the aperture, and an output signal is obtained at a time during the scan that corresponds uniquely to the radial and angular image position on the photocathode. (Bendix gives no details on the electron-ballistic description of the focusing or deflection mechanism except to cite a reference to a Farnsworth Image Dissector Tube (1939), which uses similar techniques. A brief description, taken from Reference A-4 is given at the end of this section.)

Electron Multiplier

A hollow glass tube with a high resistivity inner surface is connected through suitable applied electrodes to a voltage source of 1000 to 2000 volts, as shown in Figure A-2. A small continuous current is established along the inner surface from one end to the other; thus a uniform electric field is established down the tube. If a primary photoelectron strikes the inner surface, a secondary electron will be generated with a small transverse velocity which will tend to carry it across the tube while the longitudinal electric field accelerates it down the tube. By proper proportioning of the diameter and field strength, a sufficient amount of energy is imparted to a typical electron so that it will, on the average, generate more than one secondary upon collision with the opposite wall of the tube. Thus, a cascading action is instigated which can produce electron gain.

For this proposal Bendix chose a channel measuring $d = 0.018$ inch inside diameter and $l = 0.9$ inch in length. The resistance of the channel is approximately 10^{10} ohms; therefore, a strip current of about 2×10^{-7} ampere may be realized at 2000 volts. Output currents up to about 10^{-8} ampere may be obtained before current saturation is noticed.

Photocathode (Reference A-1 and A-3)

A semitransparent photocathode consisting of a thin film of antimony with cesium deposited on the optically treated face of the tube will be used. Its characteristics will be similar to S-11, which is tabulated in Table A-2.
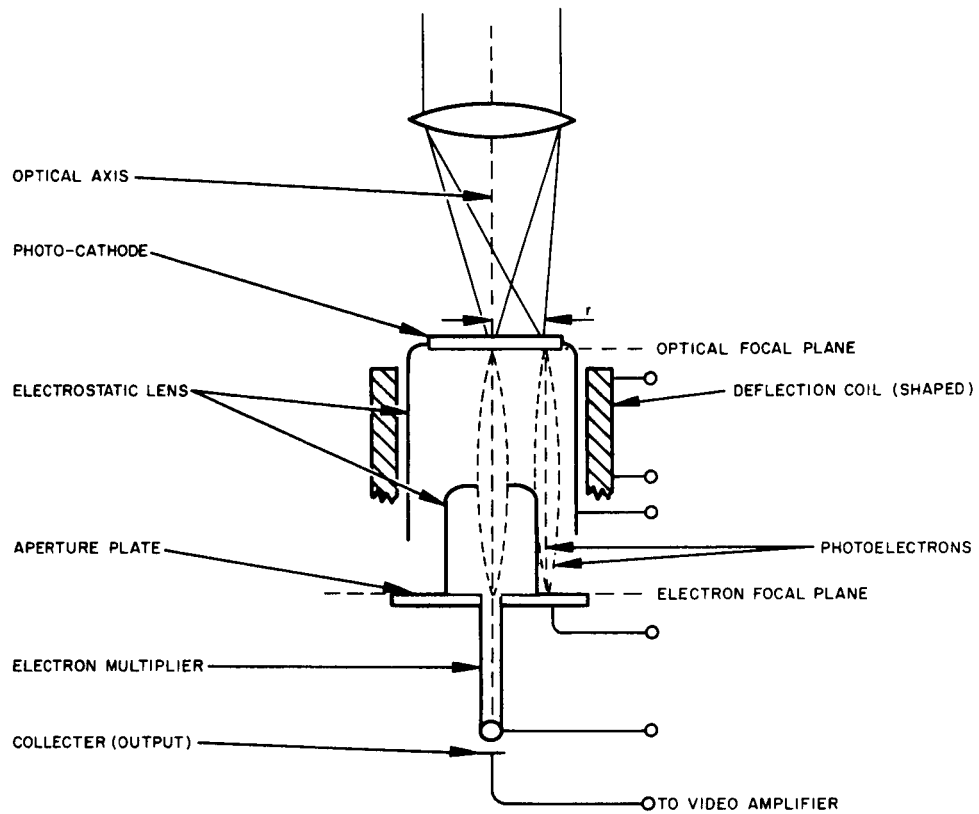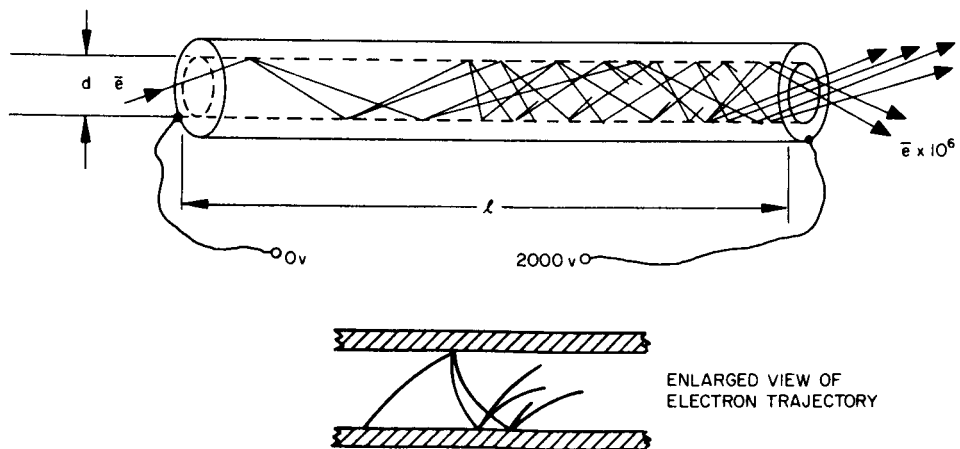
Figure A-1. Photodetector Schematic Diagram

Figure A-2. Channel Electron Multiplier

A-4

TABLE A-2. S-11 PHOTOEMISSIVE CHARACTERISTICS (CsSbO)

Radiant sensitivity at peak, S_{max}:   0.05 $\frac{\mu amp}{\mu watt}$

Wavelength at peak, λ_{max}:   4400 $\overset{o}{A}$

Luminous sensitivity: 70 $\frac{\mu amp}{lumen}$ (calibrated with 2870° K color temperature tungsten lamp)

Typical dark current emission: 10^{-14} to 10^{-15} amp/cm^2 at 25°C

10 percent response points: 3200 to 6200 $\overset{o}{A}$

Relative spectral sensitivity, S/S_{max} versus λ, $\overset{o}{A}$:

S/S_{max}	0	0.62	0.9	0.99	0.85	0.58	0.2	0.01
λ, $\overset{o}{A}$	3000	3500	4000	4500	5000	5500	6000	6500

Window: Visible light transmitting; lime glass or Kovar sealing borosilicate glass

STAR FIELD NEAR POLARIS (REFERENCE A-2 AND A-5)

In order to examine possible methods of discrimination among the stars that may appear in the 5-degree star field with Polaris, a selected star catalog whose locations are within 6 degrees declination of the north celestial pole are given in Table A-3. It should be noted that Polaris is a Cepheid variable star whose magnitude varies from 2.08 to 2.17 with a period of pulsation of 3.97 days. Thus, for design purposes the output signal-to-noise ratio of the photodetector should be based on the magnitude value of 2.17. A study of Table A-3 shows that except for Polaris there are no magnitude 2 or 3 stars in this region. The next brightest star is δ Ursa Minor which is more than 2 magnitude numbers "dimmer" than Polaris. Since the Bendix photodetector is designed for use with magnitude 3 stars or brighter, a discrimination technique based only on star brightness appears feasible. The video content of the scanned star field referenced to the sunline can be telemetered to the ground control station and displayed on a multimode (selective erasure) storage tube. Polaris can be identified by inspection or by comparison with some predetermined video level. An attitude error signal may then be generated by comparison with a superposed star field pattern (directly on the multimode storage tube face), which is driven by the local sun ephemeris

TABLE A-3. SELECTED STAR CATALOG WITHIN 6-DEGREE DECLINATION
OF NORTH CELESTIAL POLE

Name	Magnitude (Visual)	Spect.	Mean R.A. h	m	s	Mean Dec. °	'	"	Relative Order of Decreasing Brightness
Na 43 H. Cephei	4.52	KO	1	03	02.18	+86	02	56.56	3
Nbα Ursae Minoris (Polaris)	2.12 (var.)	F8	1	56	25.23	+89	04	58.05	1
Nβ Bradley 402 (Cephei)	5.78	KO	3	22	44.17	+84	46	42.74	7
Nc Groombridge 750 (Cephei)	6.7	F8	4	23	14.91	+85	26	35.42	15
Nγ B.D. +85° 74 (Cephei)	6.54	A5	5	17	45.39	+85	54	21.74	12
Nδ Groombridge 944 (Cephei)	6.41	KO	5	49	02.15	+85	10	39.62	11
Nd 51H Cephei	5.26	MO	7	22	57.90	+87	06	18.38	5
Nε Groombridge 1359 (Camelopondi)	6.39	AO	8	07	50.48	+84	10	35.02	10
Nξ B.D. +84° 196 (Camelopondi)	6.26	FO	9	07	32.67	+84	20	30.37	8
Nη B.D. +86° 161 (Camelopondi)	7.17	A2	11	10	06.69	+85	51	08.48	16
Nθ Groombridge 1850 (Camelopondi)	6.38	F5	12	02	41.06	+85	48	11.35	9
Nηδ Ursae Minoris	4.44	AO	17	44	44.67	+86	36	22.47	2
Niλ Ursae Minoris	6.55	M3	18	07	06.46	+89	03	17.19	13
Nυ Groombridge 3212 (Draconis)	6.61	A2	20	05	15.75	+84	33	31.15	14
Nξ 32 H. Cephei	5.38	AO	22	16	39.42	+85	54	46.22	6
No 36 H. Cephei	4.96	K5	22	54	47.62	+84	08	15.85	4

at the satellite longitude (with propagation delays calibrated out). Alternatively, selection and location of Polaris relative to the optical axis may be made aboard the satellite and only the location data need be telemetered. Attitude error signals may then be determined by comparing the measured data with a computed location derived from sun position and the right ascension and declination of Polaris. The former approach, however, would reduce the extra on-board electronics needed for star location at the moderate expense of additional telemetering bandwidth.

SCANNING METHODS (REFERENCE A-1)

Linear Raster Scan

In an attempt to attain precision pointing (9 seconds of arc) within a 5-degree field of view Bendix employs a coarse scan with low pointing accuracy (0.25 degree), which is switched to a fine resolution scan after the target image has been positioned to within the limit of resolution of the coarse scan. The proposed scanning system starts with a coarse linear raster in which an instantaneous field of view of 30 minutes of arc is swept over the 5-degree image field in 1/25 second. A 50-percent overlap is employed so that the image may be positioned to within 15 minutes of arc of the center of the field. When this occurs, the coarse scan is electronically switched to a small cross scan having an amplitude of 45 minutes of arc along x and y axes, centered at the origin. This produces a 30- by 30-minute overlapped field of view (from the x and y portions of the cross scan) at the center and an additional nonoverlapped 15 by 30 minutes extended along each axis, which is not used in the data processing.

Since, for the present Syncom application it is not necessary to attain a pointing accuracy much better than 0.25 degree and also, since it is desired to point the optical axis parallel to the north celestial pole and not directly at Polaris (~0.9 degree from pole), the fine scan mode will not be considered at this time.

PPI Scan

Because of the advantages of using the rotational motion of the spinning satellite to simplify the on-board sweep circuitry to one channel, a PPI scan suggests itself. Here the satellite spin angle referenced to the sun line will mechanically cause a linear, single-channel scan line (passing through the optical axis) to sweep through the star field in π radians. The frame time for a spin speed, W_s, is then

$$\text{Frame Time} = \frac{\pi}{W_s} \approx \frac{3.14}{10.5} = 0.3 \text{ second.}$$

However, the geometry yielding the spin angle location of a star may lead to some excessive spin angle ambiguity due to the apparent angular broadening (in the spin angle direction) of a star image located near the optical axis. This is caused by the constant thickness of the scan line. For example, consider a 5-degree field of view focused on a photocathode with diameter $2 r_o$. To cover adequately the periphery of the field with a 0.5-degree line scan thickness using 50-percent overlap to yield a resolution element of 0.25 degree, the equivalent spot size $\delta\varepsilon$ at the periphery of the photocathode will be approximately

$$\delta\varepsilon \ \cong \ \frac{0.25 \text{ degree}}{5 \text{ degrees}} \ 2 r_o \ = \ 0.1 \ r_o$$

The spin angle subtended by this spot size at any other distance $r < r_o$ from the tube center will be of the order

$$\frac{\delta\varepsilon}{r} \ = \ 0.1 \ \frac{r_o}{r}$$

If a star image is located a distance $r = r_o/5$ from the tube center (equivalent to a star located 1 degree from the optical axis, e.g., Polaris, when the optical axis is almost parallel to celestial pole), the spin angle subtended by the star image becomes (after five successive PPI line scans)

$$\frac{\delta\varepsilon}{r} \ = \ (0.1)(5) \frac{r_o}{r_o} \ = \ 0.5 \text{ radian} \ = \ 28.7 \text{ degrees}$$

Although this integration effect of the PPI mode enhances the signal-to-noise ratio for stars near the optical axis, some processing (such as image bisecting via angle gating of image arc) will be desirable after initial detection by the ground control equipment to facilitate the timing of precession torque pulse directions with respect to the sun line.

SOME SCAN FREQUENCY AND BANDWIDTH REQUIREMENTS

Linear Raster Scan

Scanning through a field $\theta = 5$ degrees at a frame rate of 25 frames per second with a line resolution of $\delta\theta = 0.25$ degree, the scan frequency, f_{scan}, is given by

$$\frac{1}{f_{scan}} = \tau_{scan} = \frac{\delta\theta}{\text{angle scan rate}} = \frac{\delta\theta}{\theta\,\text{frame rate}}$$

$$= \frac{0.25 \text{ degree}}{5 \text{ degrees/frame } 25 \text{ frames/second}} = 0.002 \text{ second}$$

$$f_{scan} = 500 \text{ cps}$$

For a linear sawtooth scan voltage waveform with fly-back time, $\tau_{fb} \ll \tau_{scan}$, the rate, $\delta\theta/\delta t$, at which a resolution element is scanned through may be approximated by

$$\frac{\delta\theta}{\delta t} = \frac{\theta}{\tau_{scan} - \tau_{fb}} \approx \frac{\theta}{\tau_{scan}}$$

so that the bandwidth requirement Δ_f becomes

$$\Delta f \approx \frac{1}{\delta t} \quad \frac{\theta}{\delta\theta\,\tau_{scan}} = \frac{\theta\, f^2_{scan}}{\text{angle scan rate}} = \frac{f^2_{scan}}{\text{frame rate}}$$

$$= \frac{(500)^2}{25} = 10 \text{ kc}$$

PPI Scan

Using the criteria developed earlier for peripheral coverage of the field of view, namely, for a cathode radius r_o, a field of view θ, and resolution element $\delta\theta$

$$\frac{\delta\epsilon}{2r_o} = \frac{\delta\theta}{\theta} = \frac{0.25 \text{ degree}}{5 \text{ degrees}}$$

the scan frequency f_{scan} required for a satellite spinning at a rate $\omega_s \le 13.1$ rad/sec is (nominally $\omega_s = 10.5$ rad/sec)

$$f_{scan} = \frac{\omega_s}{\delta\epsilon/r_o} \le \frac{13.1}{0.1} = 131 \text{ cps}$$

As before, the bandwidth may be determined from the rate $\delta\varepsilon/\delta t$ at which a resolution element is scanned through, i.e.,

$$\Delta f \simeq \frac{1}{\delta t} = \frac{2\,r_o}{\delta\varepsilon}\,f_{scan} = \frac{2\,f_{scan}^2}{\omega_s} \leq \frac{2(131)^2}{13.1} = 2600 \text{ cps}$$

Compared with the linear raster scan values the relatively lower f_{scan} and Δf for the PPI scan is obviously due to the inherently lower nominal frame rate of 3.3 frames per second as opposed to 25 frames per second for the raster scan. Other scan geometries and rates should be investigated.

SIGNAL-TO-NOISE RATIO CONSIDERATIONS (REFERENCE A-1)

The rms signal-to-noise ratio produced in the current delivered to the video amplifier after passing through the multiplier channel is claimed to be independent of the assumption of energy distribution of the cathode electrons. For low, dark currents (see Table A-2) and threshold signals, the theory of the shot effect in the absence of space change is applicable to determine the noise levels limiting the information content of the signal. On this basis the current signal-to-noise ratio is given by

$$\frac{i_s}{i_n} = 865 \times 10^{-m/5}\; d\left(\frac{S}{\Delta f}\;\frac{G-1}{G}\right)^{1/2}$$

where

m = astronomical magnitude of star whose image is considered
≤ 2.17 for Polaris

d = diameter of objective lens, cm

S = sensitivity of the photocathode, μ amp/μ watt
= 0.05 μ amp/μ watt for S-11 (see Table A-2)

Δf = bandwidth of signal considered
= 10 kc for linear raster scan proposed by Bendix
$\leq$ 2.6 kc for PPI scan

G = gain per electron collision with channel wall
$\simeq$ 2 for Bendix proposed design

Substituting values for m, S, and G and rearranging to solve for d gives

$$d \leq 4.46 \times 10^{-3} \left(\frac{i_s}{i_n} \right) \left(\frac{\Delta f}{0.05} \right)^{1/2}$$

Using $\Delta f = 10$ kc (raster scan) and a desired $(i_s/i_n) \cong 2$, the required objective lens diameter becomes

$$d \Big|_{\Delta f = 10 \text{ kc}} \leq 4.46 \times 10^{-3} \, (2) \left(\frac{10^4}{5 \times 10^{-2}} \right)^{1/2} = (4.46)(0.448)(2) = 4 \text{ cm}$$
$$\cong 1.575 \text{ inches}$$

For $\Delta f = 2.6$ kc (PPI scan) and $(i_s/i_n) \cong 2$

$$d \Big|_{\Delta f = 2.6 \text{ kc}} \leq 4.46 \times 10^{-3} \, (2) \left(\frac{2.6 \times 10^3}{5 \times 10^{-2}} \right)^{1/2} = (4.46)(0.228)(2) = 2.03 \text{ cm}$$
$$= 0.8 \text{ inch}$$

These values for d indicate the feasibility of using the Bendix photodetector and channel amplifier design to detect and display Polaris with reasonably sized optics.

PHYSICAL PLACEMENT AND ENVIRONMENTAL CONSIDERATIONS

No knowledge is yet available on the vibration and steady-state load factor limits of this device. A recommendation that can be made at this time is to qualify the device in the same way as an existing, physically similar Syncom component, e.g., the traveling-wave tube. To minimize the possible degrading effect of the steady-state spin load factor, the optical axis may be placed (parallel to the spin axis) at a radial distance from the spin axis that just barely prevents the 5-degree field of view from being obstructed by the antenna structure near the spin axis. The objective lens may be slightly recessed below the satellite surface structure to take advantage of spacecraft temperature control and to minimize possible lens contamination by propellant exhaust products. Similar comments apply for shading the lens from direct sunlight (where ecliptic is north of equator).

A-11

ATTITUDE REFERENCE FOR THIRD-STAGE THRUST ALIGNMENT

A launch window study is suggested to determine how often the field of view of the photodetector will contain the sun just prior to third-stage ignition. If this direct-sunlight interval does not constrain the possible launch interval too severely, a priori knowledge of the star field (associated with the preignition attitude of the third stage) may be used to finely align the third-stage thrust axis, resulting in a lower error residual of the final orbit as indicated in Reference A-6. In Advanced Syncom, for example, the out-of-plane δV_1 and in-plane δV_s velocity residuals due to thrust attitude error, $\delta \theta \cong 2$ degrees, will be reduced from nominally

$$\left| \delta V_1 \right| \cong 96 \frac{fps}{deg} \; \delta \theta = 96 \, (2) = 192 \text{ fps}$$

$$\left| \delta V_s \right| \cong 49.2 \frac{fps}{deg} \; \delta \theta = 49.2 \, (2) = 58.4 \text{ fps}$$

to about

$$\left| \delta V_1 \right| \cong 96 \, (0.25) = 24 \text{ fps}$$

$$\left| \delta V_s \right| \cong 49.2 \, (0.25) = 12.3 \text{ fps}$$

for a $\delta \theta$ of about 0.25 degree.

GENERAL CONCLUSIONS

The foregoing brief examination indicates that

1) It is feasible to adapt the Bendix photodetector for use in Syncom II to locate Polaris with reasonably sized optics.

2) Attitude error may be determined from the telemetered video content of the star field when compared with a priori ephemerides of Polaris and local sun.

3) A PPI scan geometry appears to require the simplest satellite-borne sweep circuitry.

4) Ground control video data processing, discrimination, and display techniques should be further investigated to facilitate timing of vernier control jets at the appropriate spin angle relative to the sun line.

5) Further tradeoffs between instantaneous field of view and band-
width requirements should be made to determine the bandwidth
— cost of improving resolution to, say, 0.1 degree by reducing the
collecting aperture area of the photodetector.

IMAGE DISSECTOR (NONSTORAGE) TUBE (References A-7, A-8, and A-9)

Principle of Operation

The image dissector operates on the principle of an electron-collecting
aperture which is scanned by an electron image from a photo-emitting sur-
face upon which an optical image is focused. The aperture collects the
electrons emitted by the photosensitive material of the photocathode. The
electron streams forming the electron image from the photocathode are
caused to move past the aperture by externally applied magnetic deflection
fields. The electrons collected by the aperture are introduced into the first
stage of an electron multiplier and subsequently amplified by secondary
multiplication to a sufficiently high level to develop a signal appreciably
higher than the noise generated in the following (conventional) video amplifier
stage.

The streams of electrons emitted by the photocathode of the image
dissector are brought to a focus on a plane passing through the multiplier
aperture and perpendicular to the axis of the tube. This is accomplished by
the action of an axial magnetic focusing field and the electrical field produced
by the accelerator rings. Therefore, as the entire raster is deflected across
the multiplier aperture, the aperture intercepts the sharply focused stream
of electrons produced by each illuminated area, and translates the light image
into a stream of electrons forming the video signal information. This is
illustrated by Figure A-3.

Optical Input Arrangement and Parameters

The useful area of the commercial image-dissector photocathode is a
circle of 2.75-inch diameter, permitting the use of a scanned area of 2.2 by
1.65 inches. The light from the scene to be televised is focused directly on
the photocathode, which is deposited directly on the inside of the faceplate of
the image dissector. The lens should be designed to cover this area, since
the resolution varies directly with the size of the image used on the photo-
surface.

Electrical Arrangements and Performance Characteristics

Resolution: The resolution of the image dissector is determined by
the aperture size of the collector and the magnification of the image from the
photocathode to the plane on which the image is focused. The curves of
Figure A-4 give the resolution of the tube as a function of the aperture size
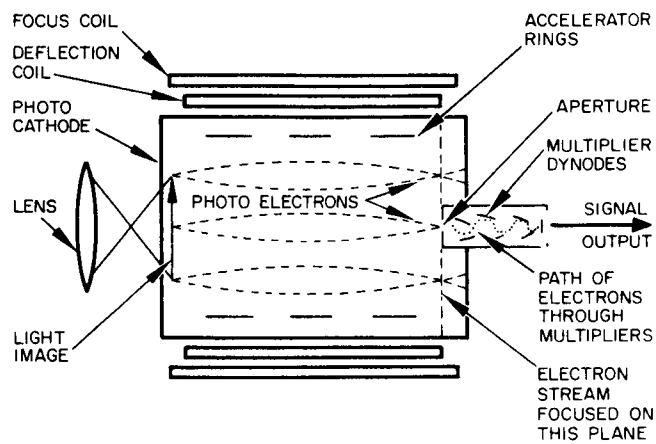(square aperture) for an image magnification of one. For different

FOCUS COIL
DEFLECTION COIL
PHOTO CATHODE
LENS
LIGHT IMAGE
PHOTO ELECTRONS
ACCELERATOR RINGS
APERTURE
MULTIPLIER DYNODES
SIGNAL OUTPUT
PATH OF ELECTRONS THROUGH MULTIPLIERS
ELECTRON STREAM FOCUSED ON THIS PLANE
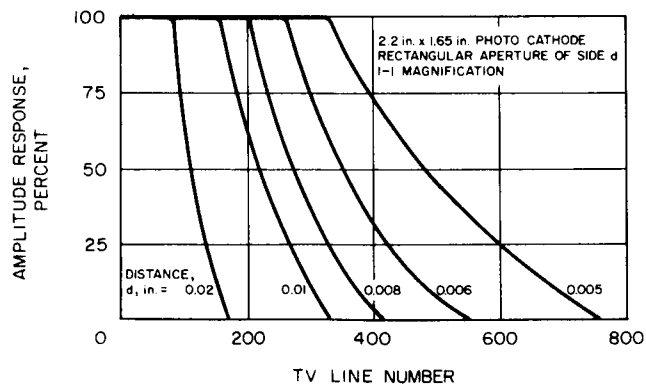
Figure A-3. Image Dissector Tube

Figure A-4. Amplitude Response of Image Dissector
as Function of Aperture Size

A-14

magnifications to the line numbers are multiplied by the magnification ratio. This curve gives the response of the tube to a square-wave test pattern in terms of peak signal amplitude and television line number.

Image dissectors are made to the specifications of the customer with respect to the size of the aperture, which ultimately controls the sensitivity and the resolving capabilities. The signal-to-noise ratio of the reproduced picture with a given illumination varies as the square root of the aperture area or directly with the aperture width. The resolution varies inversely as the width of the collecting aperture.

The signal-to-noise ratio of the signal developed can be expressed as

$$\frac{\text{peak signal}}{\text{rms noise current}} = \left(\frac{SLa(R-1)}{2Rm^2 e \, \Delta f}\right)^{1/2}$$

where

S = photosensitivity of photosurfaces, amperes per lumen

L = light intensity, foot-candles (on photosurface)

a = aperture area, square feet

m = linear magnification of image within tube

R. = secondary-emission ratio of first multiplier dynode

e = electron charge

Δ f = bandwidth, cps

The scene illumination necessary to produce this illumination on the photocathode of the tube can be determined by the following relationship

$$I_s = \frac{4f^2 L}{TR}$$

where

I_s = scene illumination, foot-candles

f = effective aperture of lens

T = transmission factor of lens

R = highlight reflectance of scene

L = illumination of photocathode

A-15

Light Transfer Characteristics: The signal output is directly propor-
tional to the input light for all signal levels below the point where the final
stages of the multiplier saturate. Saturation can be guarded against by the
use of 1) variable potentials on the multiplier stages, or 2) a controlled
multiplier stage to control the overall amplification of the multiplier. For
low-resolution systems (that is, systems employing large apertures) the
signal output will be linear up to the point where peak signal currents approach
5 milliamperes, at which point the last dynode stage tends to saturate. When
high photocurrents are drawn from the photocathode, in high-resolution tubes
where high light levels are necessary to achieve the proper signal-to-noise
ratio, saturation of the multiplier or lack of conductivity of the photosurface
may distort the picture and alter the light transfer characteristics.

Output Impedance: The multiplier of the image dissector can be con-
sidered to be a constant current generator with a very high value of shunt
impedance. The capacity to ground of the multiplier itself is 10 micromicro-
farads. Sufficient gain is obtained in the multiplier to permit the use of a
low value of load impedance. Therefore, the signal need not be corrected by
a peaking stage. The output signal can be determined by

$$I_o - \frac{SLaR^z}{m^2}$$

where

S = sensitivity of photosurface, amperes per lumen

L = illumination of surface, foot-candles

a = aperture area

z = number of stages

R = multiplier stage gain

m = magnification from photocathode to aperture

Black-level Setting: Absence of signal from the image dissector
represents black level. Black-level setting can best be achieved by shunting
the output electrode to ground during the retrace interval, producing a zero
output voltage, which represents black signal. An appropriate blanking sig-
nal is also inserted at this point to fix the blanking level with respect to the
black-level information of the picture.

Multiplier Gain: The average stage gain of the multiplier is a function
of the voltage applied across the stages. This varies between approximately
2.5 for 100 volts per stage and 4 for 200 volts per stage. The usual number
of multiplier stages is 11.

Auxiliary Circuits

Focus Coil: The use of a long-focus solenoid reduces the geometric distortion of the picture and produces unity magnification. The average field strength required is 20 gauss.

Deflection Coils: The deflection coils located adjacent to the tube and under the focus coil produce a cross component of deflection field in the order of 4 gauss for full deflection.

Focusing Electrodes: Focusing electrodes consisting of a series of rings along the path of the electron image produce a uniform accelerating field for the electron image. Connection to these electrodes is made through terminals on the periphery of the faceplate. Each of these rings is maintained approximately 100 volts positive with respect to the preceding one. The anode of the tube is maintained at ground potential and the photocathode at approximately -2000 volts, while the aperture of the multiplier is maintained at approximately -1400 volts.

REFERENCES

A-1.   "Optical Tracker," Engineering Proposal No. 9011-62-51, Sales File No. 1554, Eclipse-Pioneer Division, Bendix Corp., October 17, 1962.

A-2.   Payne-Gaposchkin, C., "Introduction to Astronomy," Chapter XIV, Prentice-Hall, 1955.

A-3.   "Typical Absolute Spectral Response Characteristics of Photoemissive Devices," Chart, ITT Components and Instrumentation Laboratory, Fort Wayne, Indiana.

A-4.   Fink, D. G., "Television Engineering Handbook," McGraw-Hill Television Series, Section 5.5, 1957.

A-5.   "Apparent Places of Fundamental Stars, 1961," Astronomisches Rechnen-Institut, Heidelberg, 1960, (under auspices of International Astronomical Union).

A-6.   "Advanced Syncom, Initial Project Development Plan," Vol. 1, Hughes Aircraft Company, SSD 2380R, 15 August 1962.

A-7.   C.C. Larson and B.C. Gardner, "The Image Dissector," Electronics Vol. 12, No. 10, pp. 24-27, 50, October 1939.

A-8.   N. Schaetti, "An Image Dissector Without Storage for Film Scanner," Bull. assoc. suisse elec., Vol. 40, No. 17, pp. 569-570, 1949.

A-9. N. Schaetti, "An Image Dissector of the Non-storage Farnsworth Type," Helv. Phys. Acta, Vol. 24, No. 2, pp. 225-232, 1949.